Coherent Structures in Nonlocal Dispersive Active-Dissipative Systems

SIAM J. APPL. MATH.
Vol. 75, No. 2, pp. 538–563

COHERENT STRUCTURES IN NONLOCAL DISPERSIVE ACTIVE-DISSIPATIVE SYSTEMS*

TE-SHENG LIN†, MARC PRADAS‡, SERAFIM KALLIADASIS§, DEMETRIOS T. PAPAGEORGIOU¶, AND DMITRI TSELUIKO‖

Abstract. We analyze coherent structures in nonlocal dispersive active-dissipative nonlinear systems, using as a prototype the Kuramoto–Sivashinsky (KS) equation with an additional nonlocal term that contains stabilizing/destabilizing and dispersive parts. As for the local generalized Kuramoto–Sivashinsky (gKS) equation (see, e.g., [T. Kawahara and S. Toh, *Phys. Fluids*, 31 (1988), pp. 2103–2111]), we show that sufficiently strong dispersion regularizes the chaotic dynamics of the KS equation, and the solutions evolve into arrays of interacting pulses that can form bound states. We analyze the asymptotic characteristics of such pulses and show that their tails tend to zero algebraically but not exponentially, as for the local gKS equation. Since the Shilnikov-type approach is not applicable for analyzing bound states in nonlocal equations, we develop a weak-interaction theory and show that the standard first-neighbor approximation is no longer applicable. It is then essential to take into account long-range interactions due to the algebraic decay of the tails of the pulses. In addition, we find that the number of possible bound states for fixed parameter values is always finite, and we determine when there is long-range attractive or repulsive force between the pulses. Finally, we explain the regularizing effect of dispersion by showing that, as dispersion is increased, the pulses generally undergo a transition from absolute to convective instability. We also find that for some nonlocal operators, increasing the strength of the stabilizing/destabilizing term can have a regularizing/deregularizing effect on the dynamics.

Key words. nonlocal partial differential equations, coherent-structure theory, solitary pulses

AMS subject classifications. 00A69, 35B41, 35Q53, 35R10, 37L15, 65P40, 76D33

DOI. 10.1137/140970033

1. Introduction.

Nonlocal models arise in a wide variety of natural phenomena and technological applications, such as optical systems [43], cell biology [4], plastic materials [59], and in many problems involving nonequilibrium interfaces, such as flame propagation and thin-film growth [37]. Some well-known examples of nonlocal partial differential equations (PDEs) are the Benjamin–Ono (BO) equation describing propagation of internal waves in a deep stratified fluid [8]; the Smith equation governing certain types of continental-shelf waves [48]; a nonlocal Korteweg–de Vries (KdV) equation describing shallow-water waves when a viscous boundary layer (on the bottom) is taken into account [23, 24, 35]; the same nonlocal KdV equation but with an additional nonlocal term to account for Marangoni effects on the free sur-

*Received by the editors May 22, 2014; accepted for publication (in revised form) January 20, 2015; published electronically March 19, 2015. This work was supported by the EPSRC under grants EP/J001740/1 and EP/K041134/1.

http://www.siam.org/journals/siap/75-2/97003.html

†Department of Applied Mathematics, National Chiao Tung University, 1001 Ta Hsueh Road, Hsinchu 300, Taiwan, and Department of Mathematical Sciences, Loughborough University, Loughborough LE11 3TU, UK (tslin@math.nctu.edu.tw).

‡Department of Mathematics and Statistics, The Open University, Milton Keynes MK7 6AA, UK, and Department of Chemical Engineering, Imperial College London, London SW7 2AZ, UK (m.pradas-gene@imperial.ac.uk).

§Department of Chemical Engineering, Imperial College London, London SW7 2AZ, UK (s.kalliadasis@imperial.ac.uk).

¶Department of Mathematics, Imperial College London, London SW7 2AZ, UK (d.papageorgiou@imperial.ac.uk).

‖Department of Mathematical Sciences, Loughborough University, Loughborough LE11 3TU, UK (d.tseluiko@lboro.ac.uk).

face [57]; a nonlocal Kuramoto–Sivashinsky (KS) equation describing nanostructuring by ion beam sputtering [14] and a wide spectrum of fluid flow problems, such as combined shear-flow and thermocapillary instabilities in two-layer systems [60] and core annular flows [38]; the nonlocal nonlinear Schrödinger equation [27]; and the nonlocal Klein–Gordon equation to describe Josephson junctions in thin films [20].

Our interest here is in the study of coherent structures in nonlocal dispersive active-dissipative equations that are characterized by the presence of instability (energy production) and stability (energy dissipation) mechanisms. As a prototype, we consider the nonlocal KS equation,

$$\partial_t u + u\partial_x u + \partial_x^2 u + \partial_x(\mathcal{N}[u]) + \partial_x^4 u = 0, \tag{1.1}$$

which is one of the simplest models to take into account the main ingredients of wave evolution in nonlinear media. $u\partial_x u$ represents the leading-order nonlinearity, $\partial_x^2 u$ the instability and energy production, and $\partial_x^4 u$ the stability and energy dissipation, and $\mathcal{N}$ is a linear nonlocal operator. Active-dissipative equations arise in a wide variety of physical problems, e.g., chemical physics to describe propagation of concentration waves [30], combustion dynamics to describe flame front instabilities [47], and falling liquid films [21, 25, 26, 32, 36]. The so-called generalized KS (gKS) equation is the local KS equation with a dispersive term of the form $\delta\partial_x^3 u$.

It is well known that solutions of many active-dissipative equations are characterized by a particular spatial and temporal behavior, e.g., by space, time, or space-time localized structures, the so-called coherent structures. For example, sufficiently large δ in the gKS equation regularizes the chaotic behavior of the KS equation, and solutions evolve into arrays of weakly interacting pulses of approximately the same shape, resembling the one-hump infinite-domain pulse (see, e.g., [2, 9, 16, 28, 51, 55, 56]). Note that the regularizing effect of dispersion has also been observed in other "local" equations, e.g., the related Nikolaevskiy equation [46]. The existence and stability of two-pulse solutions in the fifth-order KdV equation are studied in [12]. The nonlinear stability of the periodic solutions of the gKS equation has been resolved only recently [6]. For one-dimensional "local" equations with translational invariance, the dynamical systems approach can be employed to analyze pulse solutions. Indeed, spatially localized solutions can be considered as homoclinic orbits in an appropriate phase space, and the Shilnikov-type analysis can be used to analyze the existence of subsidiary homoclinic orbits [19]. Such subsidiary homoclinic orbits correspond to bound states of the pulses (i.e., multipulse solutions) of the underlying PDE.

Our aim is to analyze the effect of nonlocal terms on coherent structures. It should be noted that for nonlocal equations, the Shilnikov-type approach is not applicable, and we will therefore analyze multipulse solutions by developing a weak-interaction theory. We introduce the nonlocal linear operator $\mathcal{N}[u]$ in (1.1), and we assume that $\mathcal{N}[u]$ is a pseudodifferential operator whose symbol is independent of x. In addition, we assume that the nonlocal term has both dispersive and stabilizing/destabilizing effects. So we write

$$\mathcal{N}[u] = \delta\,\mathcal{N}_1[u] + \mu\mathcal{N}_2[u], \tag{1.2}$$

where $\delta \geq 0$, $\mu \in \mathbb{R}$, and $\mathcal{N}_1$, $\mathcal{N}_2$ are dispersive and destabilizing nonlocal linear operators, respectively. Namely, we assume that the symbols of $\mathcal{N}_1$, $\mathcal{N}_2$ are $n_1(k)$, $\mathrm{i}\,n_2(k)$, respectively, where $n_1(k)$ and $n_2(k)$ are an even and an odd real-valued function of the wavenumber k, respectively. Also, we assume $n_2(k) > 0$ for $k > 0$, so that the

positive/negative value of μ in (1.2) corresponds to the destabilizing/stabilizing effect, respectively. In addition, for the scope of the present paper we will require that $n_1(k)$ and $n_2(k)$ be continuous functions such that $|n_1(k)|$, $|n_2(k)| = o(1)$ as $k \to 0$. Then, by linearizing the equation around $u = 0$ and considering solutions of the form $u \propto \mathrm{e}^{st+\mathrm{i}kx}$, we obtain the dispersion relation

$$s(k) = k^2 - \mathrm{i}\,\delta\, k\, n_1(k) + \mu\, k\, n_2(k) - k^4, \tag{1.3}$$

from which it can be clearly seen that, indeed, the nonlocal term $\mathcal{N}_1$ introduces a dispersive effect and $\mathcal{N}_2$ introduces destabilization or stabilization depending on the sign of μ.

Let us now consider several examples. If $n_1(k) = -|k|$, we find $\partial_x(\mathcal{N}_1[u]) = \mathcal{H}[\partial_x^2 u]$, where $\mathcal{H}$ is the Hilbert transform operator defined by $\mathcal{H}[f] = \frac{1}{\pi} \int_{-\infty}^{\infty} \frac{f(\xi)}{x-\xi}\, \mathrm{d}\xi$. This type of nonlocal dispersive term appears, for example, in the BO equation. If $n_1(k) = -k^2$, we find that $\partial_x(\mathcal{N}_1[u])$ is in fact a local operator equal to $\partial_x^3 u$. In this case, if $\mu = 0$, we recover the gKS equation in which the dispersive term represents streamwise viscous-diffusion effects in the context of falling liquid films [26]. In addition, in the case when $\mu \neq 0$ and $n_2(k) = \mathrm{sgn}(k)\, k^2$, we find that $\partial_x(\mathcal{N}_2[u]) = \mathcal{H}[\partial_x^3 u]$. Such nonlocal extensions of the KS equation were derived, e.g., in [53, 54] to describe wave dynamics on electrified falling films, and the global existence and uniqueness of the solutions and the existence of the global attractor are given in [52]. The analyticity properties of solutions in a more general setting have been recently analyzed in [3]. Another example, where both $\mathcal{N}_1[u]$ and $\mathcal{N}_2[u]$ are nonlocal, is the long-wave model describing the evolution of a thin liquid film sheared by a turbulent gas [33, 50, 58].

In the long-wave approximation, when only the wavenumbers k close to zero are considered to be important, it is often appropriate to replace the symbol of a nonlocal operator by a simpler expression, e.g., by a Taylor polynomial at $k = 0$ in the case when the symbol is smooth at $k = 0$ (see, e.g., [1, 7, 49]). The approximation by a Taylor polynomial leads to localization of the nonlocal operator. Although in some cases such localization can lead to significant differences compared to the full equation (e.g., models with full dispersion in the analysis of nonlinear waves allow for breaking and peaking as opposed to the KdV equation; see [49, 61]), in many cases the qualitative characteristics of the solutions of the full nonlocal equation are the same as those of the solutions of the corresponding localized equation; see, e.g., [7, 49]. In the present study, we assume that $n_i(k) \sim k^{p_i}$ as $k \to 0^+$, $i = 1, 2$, and, considering the long-wave approximation discussed above, we replace $n_1(k)$ by $-|k|^{p_1}$ and $n_2(k)$ by $\mathrm{sgn}(k)|k|^{p_2}$. (We note that we can assume that $n_1(k)$ is nonpositive without loss of generality.) Then, $\mathcal{N}_1$ and $\mathcal{N}_2$ can be written in terms of the fractional Laplacian and the Hilbert transform operator as

$$\mathcal{N}_1[u] = -(-\partial_x^2)^{p_1/2}, \qquad \mathcal{N}_2[u] = -\mathcal{H} \circ (-\partial_x^2)^{p_2}. \tag{1.4}$$

In our study, we will assume that $p_1 > 0$ and $p_2 \in (0, 3)$ to keep fourth-order dissipation. (However, for some of the results we will find that it is necessary to additionally assume that $p_1 < 3$.) It is worth noting that fractional Laplacians are found in various applications. For example, such operators are generators of α-stable Lévi processes and arise in the study of generalized Fokker–Plank equations for stochastic differential equations driven by non-Brownian Lévi processes [34, 45]. Therefore, they are of relevance in various areas of the natural sciences.

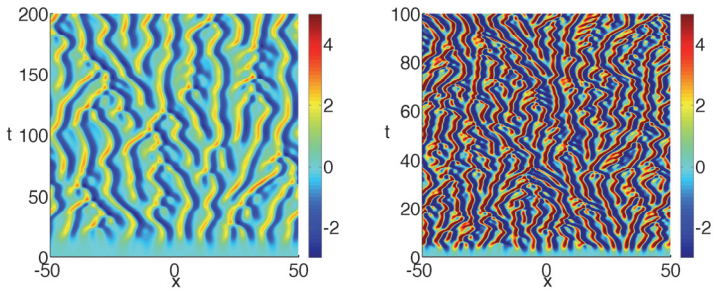

(a) $(\delta, \mu, p_1, p_2) = (0, 0, 0, 0)$.

(b) $(\delta, \mu, p_1, p_2) = (0, 1, 0, 2)$.

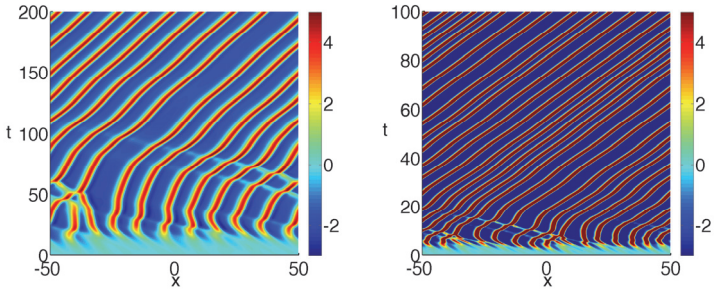

(c) $(\delta, \mu, p_1, p_2) = (1, 0, 2, 0)$.

(d) $(\delta, \mu, p_1, p_2) = (1, 1, 2, 2)$.

FIG. 1. *(Color online.) Spatio-temporal dynamics of* (1.1) *with different parameter values. Without dispersion* ($\delta = 0$)*, the dynamics is chaotic while the solution evolves into an array of pulses with strong enough dispersion* ($\delta = 1$)*. The equation is local for* (a), (c) *and is nonlocal for* (b), (d).

The rest of the paper is organized as follows. In section 2 we report numerical results on time evolution of solutions of (1.1). In section 3 we analyze the single-pulse solutions on the infinite domain. In section 4 we develop a weak-interaction theory of pulses. In section 5 we analyze the absolute and convective instability of a single-pulse solution. Finally, concluding remarks are given in section 6.

2. Spatio-temporal dynamics. To obtain a basic understanding of the dynamics, we perform numerical time simulations of (1.1) using the implicit-explicit two-step backward differentiation formula (IEBDF) given in [2]. The solutions are computed on the periodic domain $x \in [-50, 50]$ using as an initial condition a small random zero-mean perturbation to the constant state $u = 0$.

Figure 1 shows the contour plot of u corresponding to the time evolution for four different chosen parameter values. In panel (a), $\delta = \mu = 0$, which corresponds to the KS equation, and we observe the well-known chaotic dynamics of the KS equation. In panel (b), we add a destabilizing nonlocal term to the KS equation by choosing $\delta = 0$, $\mu = 1$, and $p_2 = 2$. This results in chaotic dynamics with smaller spatial and time scales. In panel (c), instead of adding a destabilizing term, we add a dispersive term by choosing $\delta = 1$, $\mu = 0$, and $p_1 = 2$, with the resulting equation being the gKS equation. In this case, the chaotic behavior is regularized by dispersion, and the solution evolves into an array of weakly interacting pulses of approximately the same shape, as noted in section 1. Finally, in panel (d), we add both the destabilizing and dispersive terms by choosing $\delta = \mu = 1$ and $p_1 = p_2 = 2$. We can again observe that

the chaotic behavior is regularized by dispersion—the solution evolves into an array of weakly interacting pulses. Also, we observe that the effect of the destabilizing term is an increase in the number of pulses in the given domain.

We aim to describe the evolution of the system as an interaction of coherent traveling-pulse structures (Figure 1(c) and (d), for example). In the following section, we will first analyze single-pulse solutions in more detail in order to quantify the basic building blocks of the pulse array.

3. Single-pulse solutions on the infinite domain. In a frame moving with velocity c, (1.1) takes the form

$$\partial_t u - c\,\partial_x u + u\partial_x u + \partial_x^2 u + \partial_x\left(\mathcal{N}[u]\right) + \partial_x^4 u = 0. \tag{3.1}$$

Let u^* denote a single-pulse solution moving at velocity c^*. It satisfies the equation

$$-c^*\partial_x u^* + u^*\partial_x u^* + \partial_x^2 u^* + \partial_x\left(\mathcal{N}[u^*]\right) + \partial_x^4 u^* = 0. \tag{3.2}$$

Integrating (3.2) and using that $u^* \to 0$ as $x \to \pm\infty$ yields

$$-c^* u^* + \frac{1}{2}u^{*2} + \partial_x u^* + \mathcal{N}[u^*] + \partial_x^3 u^* = 0. \tag{3.3}$$

Another spatial integral of (3.3) yields

$$c^* \int_{-\infty}^{\infty} u^*\,dx = \frac{1}{2}\int_{-\infty}^{\infty} u^{*2}\,dx \tag{3.4}$$

(assuming that both integrals exist), which implies that for a nontrivial solution, both the velocity of the pulse and the spatial integral of the pulse shape (i.e., the "mass" of the pulse) are not zero. Moreover, the pulse velocity can be found in terms of its shape.

We note that if the operator $\mathcal{N}$ is nonlocal, either $\mu \neq 0$ and $p_2 \neq 1$ or $\delta \neq 0$ and p_1 is not an even integer, then (3.2) cannot be written in the form of a three-dimensional dynamical system. Therefore, the pulse solutions cannot be obtained numerically in a standard way by using, e.g., the continuation software Auto07p [15]. Taking into account the fact that the nonlocal term we consider here has a simple representation in the Fourier space, we employ a spectral method and represent (3.3) on a periodic domain, $[-L, L]$, as a system for the Fourier coefficients. We then obtain pulse solutions as solutions of this system by performing continuation with respect to L and by letting L be large. We also impose a pinning condition (e.g., we set one of the Fourier coefficients to zero) to fix the translational invariance of the solution. We then use both a modified package of Auto07p and MATLAB for the computations.

First, it is known that the branch of single-pulse traveling wave solutions bifurcates from a flat solution at the critical value of the half-period, $L = L_c$ [9, 26], where a sinusoidal wave with the wavenumber $k = \pi/L$ becomes linearly unstable. We denote the critical value of the wavenumber by k_c, i.e., $k_c = \pi/L_c$. Assuming that $u = \alpha + \beta e^{st+ikx}$, where $|\beta| \ll 1$, one finds the following dispersion relation after substituting this in (3.1):

$$s(k) = i\,c\,k - i\,u_0\,k + k^2 + i\,\delta\,k\,|k|^{p_1} + \mu\,|k|^{p_2+1} - k^4. \tag{3.5}$$

The condition that the growth rate is zero determines k_c, i.e., $k_c^2 + \mu\,|k_c|^{p_2+1} - k_c^4 = 0$. Note that we are interested only in the positive solution. For example, for $\mu = 0$, we

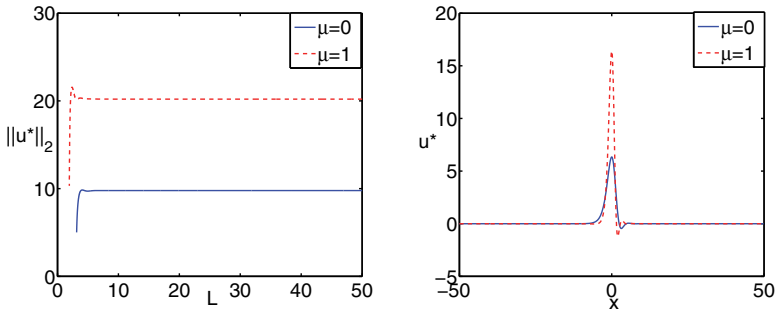

(a) Continuation with respect to L. (b) Pulse solutions at $L = 50$.

FIG. 2. *(Color online.) One-hump pulse solutions for* $\delta = 1$, $p_1 = p_2 = 2$.

obtain $k_c = 1$. The frame speed c^* in which the wave does not propagate either to the left or to the right is determined by the condition $\mathrm{Im}(s(k)) = 0$, which implies $c^* = \alpha - \delta\,|k|^{p_1}$. When k is close to k_c, we obtain $c^* = \alpha - \delta\,k_c^{p_1}$ to leading order. Next, when the integrations are from $-L$ to L, condition (3.4) gives to leading order $c^* = \alpha/2$. Solving this equation together with the previous one, we obtain that near the critical value of the period the speed of an infinitesimal sinusoidal wave is to leading order $c^* = \delta\,k_c^{p_1}$, and such a wave bifurcates from the flat solution of thickness $\alpha = 2\,\delta\,k_c^{p_1}$. We start the continuation by using the periodic domain for which L is slightly bigger than $L_c = \pi/k_c$ and using a small-amplitude sinusoidal perturbation to the flat solution $u = \alpha$ as an initial guess. The results of numerical continuation are shown in Figure 2(a) for $\delta = 1$, $p_1 = p_2 = 2$, and $\mu = 0$ and 1 by the solid (blue) and dashed (red) lines, respectively. We choose the L^2-norm $\|u^*\|_2 = (\int_{-L}^{L} u^{*2}\,\mathrm{d}x)^{1/2}$ as the measure of the solution. We observe that as L increases, $\|u^*\|_2$ converges to a constant value. The corresponding pulse solutions at $L = 50$ are shown in Figure 2(b). We note that the pulse amplitude is larger for the larger value of μ.

Next we fix the domain size by choosing $L = 50$ and perform continuation on the parameters of the equation. Figure 3 depicts bifurcation diagrams showing the dependence of the pulse velocity c^* on δ when $p_1 = p_2 = 2$ with $\mu = 0$ and $\mu = 1$. Panel (a) shows the range $\delta \le 2$, while panel (b) shows the range $1 \le \delta \le 200$ on a log-log scale. The solid (blue) and the dashed (red) lines correspond to $\mu = 0$ and 1, respectively. In panel (a) the diagram is characterized by a snaking behavior near $\delta = 0$ so that there exists a multiplicity of solutions for sufficiently small values of δ. However, only the upper parts of both diagrams correspond to one-hump pulse solutions that are the main feature of the large-time evolution. On the other hand, in panel (b) we observe that for large values of δ, the pulse speeds are linearly proportional to δ, and the proportionality constant is larger for a larger value of μ.

Figure 4 depicts bifurcation diagrams showing the dependence of the pulse velocity c^* on μ when $\delta = 1$. The solid (blue), dashed (red), and broken (green) lines correspond to $(p_1, p_2) = (2, 2)$, $(p_1, p_2) = (1, 2)$, and $(p_1, p_2) = (2, 1.5)$, respectively. In all cases c^* is an increasing function of μ. Panel (b) shows the results on the log-log scale, and it can be seen that the pulse velocities scale as $O(\mu^2)$ for $p_2 = 1.5$ and $O(\mu^3)$ for $p_2 = 2$. We also find that the scalings are independent of the value of p_1. For example, the lines for $(p_1, p_2) = (1, 2)$ and $(p_1, p_2) = (2, 2)$ collapse for large μ.

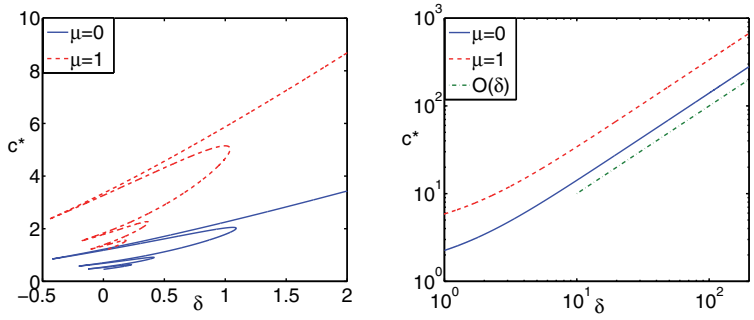

(a) (b)

FIG. 3. *(Color online.) Continuation of the pulse solutions with respect to* δ *for* $p_1 = p_2 = 2$ *and* $L = 50$. *Panel* (a) *shows the range* $\delta \leq 2$, *and panel* (b) *shows the range* $1 \leq \delta \leq 200$ *on a log-log scale.*

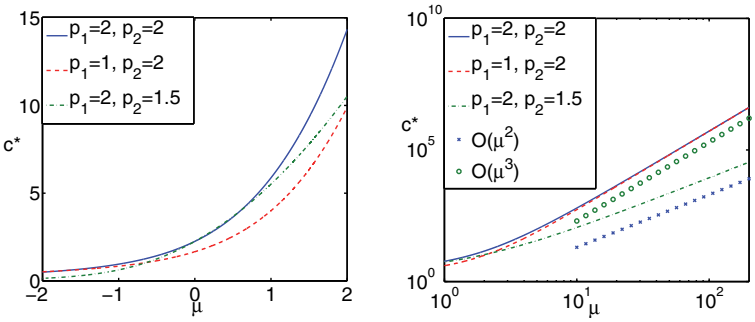

(a) (b)

FIG. 4. *(Color online.) Continuation of the pulse solutions with respect to* μ *for* $\delta = 1$ *and* $L = 50$. *Panel* (a) *shows the range* $\mu \leq 2$, *and panel* (b) *shows the range* $1 \leq \mu \leq 200$ *on the log-log scale.*

Next we analyze the profiles of single-pulse solutions. In Figure 5, $\delta = 1$, $\mu = 0$, and p_1 varies. As can be seen in panel (a), the pulse amplitude increases as p_1 increases. In panel (b), we show the semilog plots of the absolute values of the pulse solutions. It is found that the right and left tails of the pulse decay exponentially only for $p_1 = 2$; see also panel (c) showing the absolute values of the pulse tails on the semilog scale. For $p_1 \in (0, 3) \setminus \{2\}$, we can observe that both tails decay algebraically. This is further demonstrated by plotting the absolute values of the pulse solutions on a log-log scale; see panel (d), for example, for the case $p_1 = 1.5$. Interestingly, for $p_1 = 1.5$ we find that the tails decay as $1/|x|^{2.5}$ when $x \to \pm\infty$. In fact, from our simulations, we can conclude that the tails decay as $1/|x|^{p_1+1}$, and the rate of the decay is independent of the magnitude of δ. We have also found a similar scenario when the nonlocal $\mathcal{N}_2$ term is present. For $\delta = 0$ and $\mu \neq 0$, the tails decay as $1/|x|^{p_2+1}$ (with the exception of $p_2 = 1$, which corresponds to a local equation).

3.1. Large δ limit. To gain insight into the pulse characteristics for large δ we invoke scaling arguments. For increasing values of δ a balance in (3.2) must take place between the dispersive nonlocal term $\delta\,\partial_x(\mathcal{N}_1[u^*])$, the nonlinearity $u^*\partial_x u^*$, and the term $c^*\partial_x u^*$. We therefore have $\delta\, U \sim U^2 \sim c^*\, U$, where U denotes the scale for

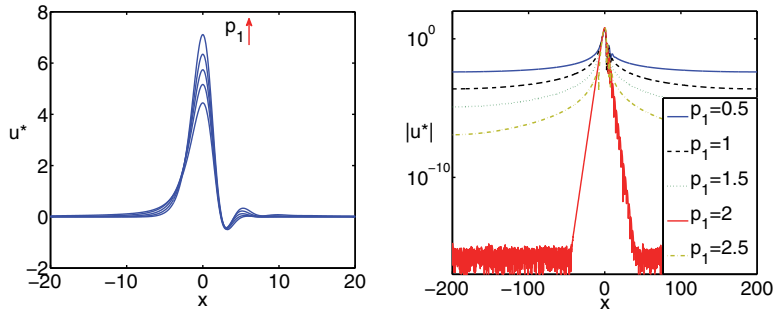

(a) $\delta = 1$, $\mu = 0$ with various p_1. (b) $\delta = 1$, $\mu = 0$ with various p_1.

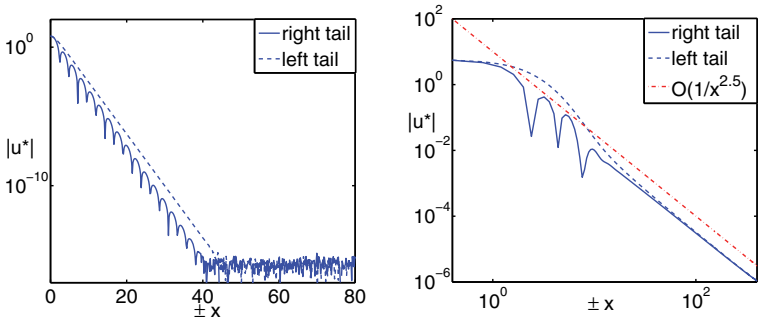

(c) $\delta = 1$, $\mu = 0$, $p_1 = 2$. (d) $\delta = 1$, $\mu = 0$, $p_1 = 1.5$.

FIG. 5. *(Color online.) Panels* (a) *and* (b) *show single-pulse solutions of* (3.3) *for* $\delta = 1$, $\mu = 0$, *and* $p_1 = 0.5$, 1, 1.5, 2, *and* 2.5 *on normal and semilog scales, respectively.* (c) *A single-pulse solution with exponentially decaying tails shown on a semilog scale.* (d) *A single-pulse solution with algebraically decaying tails shown on a log-log scale. The asymptote,* $1/x^{2.5}$, *is shown as a dotted (red) line.*

the pulse amplitude. This implies that $U \sim \delta$ and $c^* \sim \delta$. We then utilize the asymptotic expansions $u^* = \delta u_0 + u_1 + \cdots$, $c^* = \delta c_0 + c_1 + \cdots$, and by substituting these expansions in (3.3), we obtain the following equation at leading order:

$$-c_0 u_0 + \frac{1}{2}u_0^2 + \mathcal{N}_1[u_0] = 0. \tag{3.6}$$

For $p_1 = 1$ or 2, this is the equation for determining traveling-wave or pulse solutions of the BO or KdV equation, respectively. For both the BO and the KdV equation, analytical solutions are known, namely, $u_0 = 4c_0/(c_0^2 x^2 + 1)$ and $u_0 = 3c_0 \operatorname{sech}^2(\sqrt{c_0}\, x/2)$, respectively. In both cases, there is a continuous dependence of the pulse shape on c_0, and c_0 is therefore not uniquely determined. This is in fact the case for any $p_1 > 0$ due to the following scaling symmetry of the equation: With the scalings $u_0 = c_0\, \bar{u}_0$ and $x = c_0^{-1/p_1}\, \bar{x}$, (3.6) can be rewritten as

$$-\bar{u}_0 + \frac{1}{2}\bar{u}_0^2 + \mathcal{N}_1[\bar{u}_0] = 0, \tag{3.7}$$

and we can therefore write $u_0 = c_0\, \bar{u}_0(c_0^{1/p_1} x)$. (Here we used the fact that $\mathcal{N}_1[f](x) = X^{-p_1}\mathcal{N}_1[\tilde{f}](\tilde{x})$, where $\tilde{f}(\tilde{x}) = f(X\tilde{x})$ and X is a positive constant.)

To determine the constant c_0, we note that the equation at first order is

$$-c_0 u_1 + u_0 u_1 + \mathcal{N}_1[u_1] = c_1 u_0 - \partial_x u_0 - \mu \mathcal{N}_2[u_0] - \partial_x^3 u_0. \tag{3.8}$$

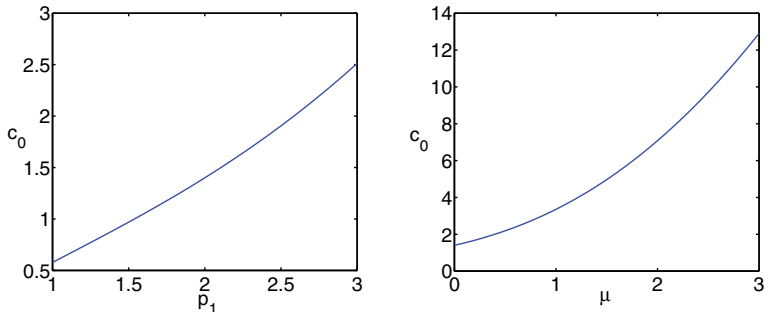

(a) $\mu = 0$. (b) $p_1 = 2$ and $p_2 = 2$.

FIG. 6. *The proportionality constant* c_0 *obtained by solving* (3.10) *as a function of* (a) p_1 *and* (b) μ.

The Fredholm alternative solvability condition on u_1 implies that the inner product of $\partial_x u_0$ with the right-hand side of (3.8) should vanish, which leads to

$$\int_{-\infty}^{\infty} [(\partial_x u_0)^2 + \mu \partial_x u_0 \mathcal{N}_2[u_0] - (\partial_x^2 u_0)^2] \, \mathrm{d}x = 0. \tag{3.9}$$

This condition determines c_0. Substituting $u_0 = c_0 \, \bar{u}_0(c_0^{1/p_1} x)$ in (3.9), we obtain

$$c_0^{2+1/p_1} A + \mu \, c_0^{2+p_2/p_1} B - c_0^{2+3/p_1} C = 0, \tag{3.10}$$

where $A = \int_{-\infty}^{\infty} (\partial_{\bar{x}} \bar{u}_0)^2 \, \mathrm{d}\bar{x}$, $B = \int_{-\infty}^{\infty} \partial_{\bar{x}} \bar{u}_0 \mathcal{N}_2[\bar{u}_0] \, \mathrm{d}\bar{x}$, and $C = \int_{-\infty}^{\infty} (\partial_{\bar{x}}^2 \bar{u}_0)^2 \, \mathrm{d}\bar{x}$. We note that $A > 0$, $C > 0$, and by using the properties given in Appendix A, it can be shown that $B > 0$.

For the case $\mu = 0$, we obtain $c_0 = (A/C)^{p_1/2}$. In particular, for the KdV case, when $p_1 = 2$, we obtain the well-known result $c_0 = 7/5$ (see, e.g., [9]), and for the BO case, when $p_1 = 1$, we find $c_0 = 1/\sqrt{3}$. The dependence of c_0 on p_1 is shown in Figure 6(a) for the case $\mu = 0$. For nonzero μ, (3.10) needs to be solved numerically. The dependence of c_0 on μ for $p_1 = 2$ and $p_2 = 2$ is shown in Figure 6(b), which shows that c_0 is a monotonically increasing function of μ. Remarkably, for the case $p_1 = 1$, $p_2 = 2$, the following analytical expression for the dependence of c_0 on μ can be found: $c_0 = \mu/4 + \sqrt{9\mu^2 + 48}/12$.

3.2. Large μ limit. The pulse characteristics for large values of μ can also be understood by using scaling arguments. The dominant balances in (3.2) for large μ are between the destabilizing nonlocal term $\mu \partial_x(\mathcal{N}_2[u^*])$ and the stabilizing term $\partial_x^4 u^*$ along with the nonlinearity $u^* \partial_x u^*$ and the linear term $c^* \partial_x u^*$. We therefore obtain $\frac{\mu U}{X^{p_2+1}} \sim \frac{U}{X^4} \sim \frac{U^2}{X} \sim \frac{c^* U}{X}$, where U denotes the scale for the pulse amplitude and X denotes the scale for the spatial variable x. This implies that $X \sim \mu^{-1/(3-p_2)}$, $U \sim \mu^{3/(3-p_2)}$, $c^* \sim \mu^{3/(3-p_2)}$. Similar large μ scalings have been presented in [52] for unsteady chaotic dynamics. Since $p_2 < 3$, we can conclude that as μ increases, the amplitude and speed of the pulse increase as $\mu^{3/(3-p_2)}$, whereas the spatial scale decreases as $\mu^{-1/(3-p_2)}$. These results are consistent with the numerical results for $p_2 = 1.5$ and $p_2 = 2$ presented in Figure 4(b), where we find that the pulse velocities scale as μ^2 and μ^3, respectively.

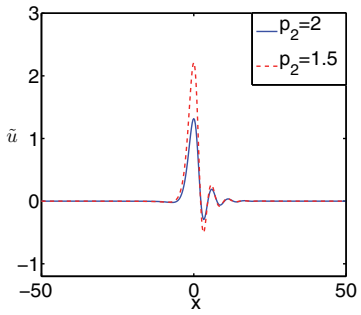

FIG. 7. *(Color online.) Single-pulse solution of* (3.12) *for* $p_2 = 2$ *(solid (blue) line) and* $p_2 = 1.5$ *(dashed (red) line).*

With the rescalings $x = \mu^{-1/(3-p_2)}\tilde{x}$, $u^*(x) = \mu^{3/(3-p_2)}\tilde{u}(\tilde{x})$, $c^* = \mu^{3/(3-p_2)}\tilde{c}$, (3.3) takes the form

$$-\tilde{c}\,\tilde{u} + \frac{1}{2}\,\tilde{u}^2 + \mu^{-\frac{2}{3-p_2}}\,\partial_{\tilde{x}}\tilde{u} + \delta\,\mu^{\frac{p_1-3}{3-p_2}}\,\mathcal{N}_1[\tilde{u}] + \mathcal{N}_2[\tilde{u}] + \partial_{\tilde{x}}^3\tilde{u} = 0, \tag{3.11}$$

indicating that the suggested scales are valid for $p_1, p_2 < 3$, and at leading order we have

$$-\tilde{c}\,\tilde{u} + \frac{1}{2}\,\tilde{u}^2 + \mathcal{N}_2[\tilde{u}] + \partial_{\tilde{x}}^3\tilde{u} = 0, \tag{3.12}$$

for which, unlike for the BO and KdV equations, an analytical form of the solution is not known. Therefore it must be solved numerically in order to determine the leading-order pulse shape and velocity. As an example, Figure 7 shows the single-pulse solutions of (3.12) for $p_2 = 2$ and $p_2 = 1.5$ that are found using a pseudospectral method together with Newton's iterations to obtain solutions from initial guesses. Unlike the BO and KdV equations, there is no continuous dependence of the solution on $\tilde{c}$; i.e., a one-hump solution is unique and $\tilde{c}$ is determined uniquely (although there may exist a countable number of other solutions of different shapes). This can be understood by the fact that there do not exist appropriate scalings to absorb $\tilde{c}$. Finally, $\tilde{c}$ and $\tilde{u}$ are independent of δ and p_1. This also coincides with our numerical observation in Figure 4(b), where we establish that the two curves, for $(p_1, p_2) = (2, 2)$ and $(p_1, p_2) = (1, 2)$, collapse onto each other for large values of μ.

3.3. Asymptotic behavior of the tails of a single-pulse solution. If the operator $\mathcal{N}$ is local, i.e., $\mu = 0$ and p_1 is an even integer, the asymptotic behavior of a single-pulse solution as $x \to \pm\infty$ can be determined by rewriting the equation as a dynamical system in an N-dimensional phase space, where $N = \max\{3, p_1\}$, and analyzing the stability of the fixed point corresponding to the origin. The decay of the tails is then found to be exponential (unless there are zero roots of the characteristic equation), and the rates and the nature (monotonic or oscillatory) of the decay are determined by the roots of the characteristic equation; see, e.g., [29] for the analysis for the gKS equation. We remark here that for local equations that have pulses with exponentially decaying tails, coherent structure theories have been developed in [5, 9, 16, 39, 40, 41, 42, 51, 55, 56].

If $\mathcal{N}$ is nonlocal, the dynamical-systems approach is not applicable. Nevertheless, the asymptotic behavior of the tails of a pulse can still be determined. First, we recall

that

$$\mathcal{F}[\mathcal{N}_1[u^*]] = -|k|^{p_1}\widehat{u^*}(k), \qquad \mathcal{F}[\mathcal{N}_2[u^*]] = \mathrm{i}\,\mathrm{sgn}(k)|k|^{p_2}\widehat{u^*}(k). \tag{3.13}$$

Here hats and $\mathcal{F}$ denote the Fourier transforms; see Appendix A. Since $\widehat{u^*}(0) = \int_{-\infty}^{\infty} u^*(x)\,\mathrm{d}x$ and we know from (3.4) that this integral is nonzero, we have, for $|k| \ll 1$,

$$\mathcal{F}[\mathcal{N}_1[u^*]] = -|k|^{p_1}\widehat{u^*}(0) + \text{h.o.t.}, \qquad \mathcal{F}[\mathcal{N}_2[u^*]] = \mathrm{i}\,\mathrm{sgn}(k)|k|^{p_2}\widehat{u^*}(0) + \text{h.o.t.}, \tag{3.14}$$

where h.o.t. denotes higher-order terms in $|k|$. Using Theorem 19 from [31, p. 52], we can conclude that as $x \to \pm\infty$,

$$\mathcal{N}_1[u^*] \sim -\frac{2\,\widehat{u^*}(0)\,\Gamma(p_1+1)\cos\big((p_1+1)\pi/2\big)}{(2\pi)^{p_1+1}}\,\frac{1}{|x|^{p_1+1}}, \tag{3.15}$$

$$\mathcal{N}_2[u^*] \sim -\frac{2\,\widehat{u^*}(0)\,\Gamma(p_2+1)\sin\big((p_2+1)\pi/2\big)}{(2\pi)^{p_2+1}}\,\frac{\mathrm{sgn}(x)}{|x|^{p_2+1}}. \tag{3.16}$$

By balancing the leading-order terms c^*u^* and $\mathcal{N}[u^*]$ in (3.3), we obtain the following cases.

Case 1. If $\mu = 0$ or $p_1 < p_2$, we find $u^* \propto -\cos\big((p+1)\pi/2\big)/|x|^{p+1}$ as $x \to \pm\infty$. Here and below we denote $p = \min\{p_1, p_2\}$. In this case, the tails of the pulse are either both positive or both negative for sufficiently large values of $|x|$, depending on whether $p \in (4k, 4k+2)$ or $p \in (4k+2, 4k+4)$, $k = 0, 1, 2, \ldots$, respectively. Here and everywhere else we assume that $\widehat{u^*}(0) > 0$.

Case 2. If $\delta = 0$ or $p_2 < p_1$, we find $u^* \propto -\sin\big((p+1)\pi/2\big)\,\mathrm{sgn}(x)/|x|^{p+1}$ as $x \to \pm\infty$. If $p \in (0,1)$, the left tail is positive, whereas the right tail is negative for sufficiently large values of $|x|$. However, if $p \in (1,3)$, the left tail is negative, whereas the right tail is positive for sufficiently large values of $|x|$.

Case 3. If μ and δ are nonzero and $p_1 = p_2$, we find that $u^* \propto -D_\pm/|x|^{p+1}$ as $x \to \pm\infty$, where $D_\pm = \delta\cos\big((p+1)\pi/2\big) \pm \mu\sin\big((p+1)\pi/2\big)$. Here we assumed $D_\pm \neq 0$.

Case 4. If μ and δ are nonzero, $p_1 = p_2$, and, in addition, either $D_- = 0$ or $D_+ = 0$, the leading-order contributions of the nonlocal $\mathcal{N}_1$ and $\mathcal{N}_2$ terms cancel each other, and we find that the left/right tail tends to zero faster than the right/left tail for $D_- = 0$ or $D_+ = 0$, respectively.

Our analytical results for the tail behavior agree with the numerical observations; see Figure 5.

4. Weak-interaction theory for solitary pulses. In this section we analyze the interaction dynamics of the pulse solutions and formation of bound states. For nonlocal equations the Shilnikov-type approach is not applicable, as discussed in section 1. We therefore analyze bound states by utilizing a weak-interaction theory. We assume that the solutions are represented by pulses that are well-separated and slowly attract and repel each other. The appropriateness of representing the solutions as arrays of pulses for certain parameter values is motivated by the time-dependent simulations presented in section 2 (see Figure 1) . In section 5, we additionally provide an analysis of absolute and convective instabilities of pulse solutions which reveals the regions of the parameter values for which the solutions evolve into arrays of pulses.

First, we consider the equation on an infinite domain and assume that the solution is described as a superposition of n well-separated quasi-stationary pulses and a small

correction function $\hat{u}(x,t)$, i.e., $u = \sum_{i=1}^{n} u_i + \hat{u}$, where u_i is a pulse located at $x_i(t)$, namely, $u_i(x,t) = u^*(x - x_i(t))$. We assume that $x_i < x_j$ for $i < j$, and we denote the separation distances by $l_i = x_{i+1} - x_i$, $i = 1, \ldots, n-1$. Substituting such an ansatz in (3.1) written in a frame moving at velocity c^* of an infinite-domain pulse, we obtain

$$\begin{aligned} &\partial_t \hat{u} - c^* \partial_x \hat{u} + \hat{u} \partial_x \hat{u} + \partial_x^2 \hat{u} + \partial_x(\mathcal{N}[\hat{u}]) + \partial_x^4 \hat{u} \\ &\quad - \sum_{i=1}^{n} \dot{x}_i \, \partial_x u_i + \sum_{\substack{i,j=1 \\ i<j}}^{n} \partial_x(u_i u_j) + \sum_{i=1}^{n} \partial_x(u_i \hat{u}) = 0, \end{aligned} \tag{4.1}$$

where the dots over the x_i's denote differentiation with respect to time. Note that we have used the fact that each u_i satisfies (3.2). For each $k = 1, \ldots, n$, we rewrite this equation as

$$\partial_t \hat{u} = \mathcal{L}_k[\hat{u}] + \sum_{i=1}^{n} \dot{x}_i \, \partial_x u_i - \sum_{\substack{i,j=1 \\ i<j}}^{n} \partial_x(u_i u_j) - \sum_{\substack{i=1 \\ i \neq k}}^{n} \partial_x(u_i \hat{u}) - \hat{u} \partial_x \hat{u}, \tag{4.2}$$

where $\mathcal{L}_k$ is the linear differential operator

$$\mathcal{L}_k[f] = c^* \partial_x f - \partial_x^2 f - \partial_x(\mathcal{N}[f]) - \partial_x^4 f - \partial_x(u_k f), \tag{4.3}$$

with the formal adjoint operator in L^2 given by

$$\mathcal{L}_k^{adj}[f] = -c^* \partial_x f - \partial_x^2 f + \mathcal{N}^{adj}[\partial_x f] - \partial_x^4 f + u_k \partial_x f. \tag{4.4}$$

Here $\mathcal{N}^{adj} = \mathcal{N}_1 - \mathcal{N}_2$ is the formal adjoint of $\mathcal{N} = \mathcal{N}_1 + \mathcal{N}_2$; see Appendix A.

As for the gKS equation (see [51, 56]), it can be shown that the spectrum of $\mathcal{L}_k$ on an infinite domain consists of two parts: the essential spectrum, given by

$$\Sigma = \{\sigma \in \mathbb{C} : \ \sigma = \mathrm{i}\, c^* \kappa + \kappa^2 + \mathrm{i}\, \delta \kappa |\kappa|^{p_1} + \mu |\kappa|^{p_2+1} - \kappa^4, \ \kappa \in \mathbb{R}\}, \tag{4.5}$$

and the two eigenvalues, one being negative and isolated and the other being equal to zero. Note that the zero eigenvalue is embedded into the essential spectrum. Observing that [18]

$$\mathcal{L}_k[\partial_x u_k] = 0, \quad \mathcal{L}_k[-1] = \partial_x u_k, \tag{4.6}$$

we conclude that the zero eigenfunction is $\partial_x u_k$ and is associated with the translational symmetry of the equation. Furthermore, on a periodic domain, zero is an eigenvalue of algebraic multiplicity 2 and geometric multiplicity 1 with the generalized eigenfunction equal to -1 that is associated with the Galilean invariance of the equation.

Our aim is to project the dynamics onto the translational modes, i.e., onto the null spaces of operators $\mathcal{L}_k$. (Note that it can be shown that the Galilean modes are never excited; see [51].) To do this, we first need to compute the null space of the adjoint operator $\mathcal{L}_k^{adj}$. To clarify the structure of the spectrum on an infinite domain, it is appropriate to consider periodic domains and take the limit when the domain size tends to infinity [44]. It turns out that on a periodic domain the zero eigenfunction of $\mathcal{L}_k^{adj}$ is a constant and the generalized eigenfunction is a function that, as the domain size increases, tends to a function approaching two different constants at $\pm\infty$ (it is precisely this function that should be used for projections onto the translational modes). This is analogous to the gKS equation [51, 56]; see

Appendix B for more details. Let us denote this function by Ψ_k. This function can be expressed as $\Psi_k = \int_{a_k}^{x} \psi_k \, \mathrm{d}x$, where ψ_k is a function of a nonzero "mass" that tends to zero algebraically as $1/|x|^{(p+1)}$ as $x \to \pm\infty$, unlike for the gKS equation where the tails decay exponentially. The point a_k is chosen so that $\int_{a_k}^{\infty} \psi_k \, \mathrm{d}x = \int_{-\infty}^{a_k} \psi_k \, \mathrm{d}x$. Note that the two functions Ψ_k and ψ_k are uniquely determined by normalization $\int_{-\infty}^{\infty} \Psi_k \partial_x u_k \, \mathrm{d}x = -\int_{-\infty}^{\infty} \psi_k u_k \, \mathrm{d}x = 1$, which leads to the conditions $\int_{-\infty}^{\infty} \psi_k \, dx = -1/c^*$, $\lim_{x\to\pm\infty} \Psi_k(x) = \mp 1/2c^*$.

Since the zero eigenvalue is embedded into the essential spectrum, rigorous projections are not well defined. We also note that the zero eigenvalue cannot be made isolated by shifting the essential spectrum to the left by utilizing exponentially weighted spaces, unlike for the gKS equation (see [56, 51]). Indeed, since the Fourier transform is defined on the Schwartz class of tempered distributions $\mathcal{S}'(\mathbb{R})$ (see, e.g., [13]), which does not contain functions that grow exponentially at positive or negative infinity, the nonlocal operator $\mathcal{N}$ given in section 1 is also defined on $\mathcal{S}'(\mathbb{R})$ and is undefined for functions growing exponentially at positive or negative infinity. Nevertheless, we can still formally introduce the "projection" operators $\Pi_k[f] = \int_{-\infty}^{\infty} f\Psi_k \, \mathrm{d}x$. Assuming that $\hat{u}$ is free of translational modes, i.e., $\Pi_k(\hat{u}) = 0$, for each $k = 1, \ldots, n$, and applying projections Π_k to (4.2), we obtain

$$\begin{aligned} \dot{x}_k = &\sum_{\substack{i,j=1 \\ i<j}}^{n} \Pi_k(\partial_x(u_i u_j)) + \sum_{\substack{i=1 \\ i\neq k}}^{n} \Pi_k(\partial_x(u_i \hat{u})) + \Pi_k(\hat{u}\partial_x \hat{u}) \\ &- \sum_{\substack{i=1 \\ i\neq k}}^{n} \dot{x}_i \Pi_k(\partial_x u_i) - \dot{x}_k \Pi_k(\partial_x \hat{u}), \end{aligned} \tag{4.7}$$

where we have used $\Pi_k(\partial_x u_k) = 1$, $\Pi_k(\partial_t \hat{u}) = -\dot{x}_k \Pi_k(\partial_x \hat{u})$, and $\Pi_k(\mathcal{L}_k[\hat{u}]) = 0$. We note that conditions $\Pi_k(\hat{u}) = 0$ can be considered as a system of equations to determine the pulse locations, $\int_{-\infty}^{\infty} (u - \sum_{i=1}^{n} u_i) \, \Psi_k \, \mathrm{d}x = 0$.

Assuming that the correction function is small, $|\hat{u}| = O(\epsilon)$, where $\epsilon \ll 1$, we rewrite (4.7) as

$$\dot{x}_k = \sum_{\substack{i,j=1 \\ i<j}}^{n} P(x_i - x_j) - \sum_{\substack{i=1 \\ i\neq k}}^{n} \dot{x}_i G(x_i - x_k) + o(\epsilon), \tag{4.8}$$

where

$$P(l) = -\int_{-\infty}^{\infty} u^*(x-l)u^*(x)\psi(x)\, dx, \quad G(l) = -\int_{-\infty}^{\infty} u^*(x-l)\psi(x)\, dx, \tag{4.9}$$

and $\psi(x)$ is such that $\psi_k(x,t) = \psi(x - x_k(t))$. Next, we assume that the pulses are well-separated with small overlap, so that $l_{min} = \min_{1\le i\le n-1}\{l_i\} = O(\epsilon^{-1/(p+1)})$. Then it follows that $\dot{x}_k$ is $O(\epsilon)$, and (4.8) takes the following form at leading order:

$$\dot{x}_k = \sum_{|x_i - x_k| < b(\epsilon)} P(x_i - x_k), \tag{4.10}$$

where we choose $b(\epsilon) \gg \epsilon^{-1/(p+1)}$.

To obtain a quantitative estimate on the appropriate separation distance and for a fixed small value of ϵ, we note that, in addition to the condition $l_{min} =$

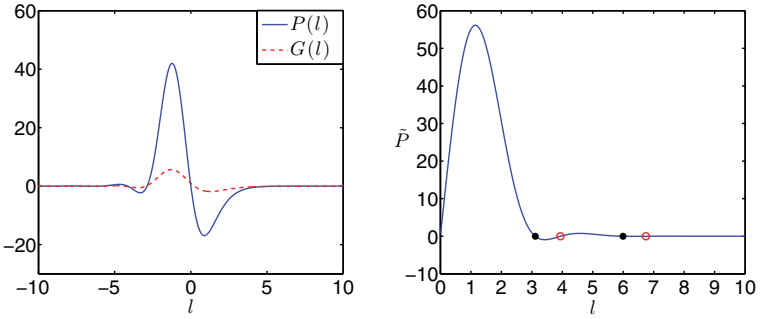

(a) $P(l)$ and $G(l)$. (b) $\tilde{P}(l) = P(-l) - P(l)$.

FIG. 8. *(Color online.) The functions* (a) $P(l)$, $G(l)$ *and* (b) $P(-l) - P(l)$ *for* $(\delta, \mu, p_1, p_2) = (1, 1, 2, 2)$. *In* (b)*, filled/empty circles indicate stable/unstable equilibria, respectively.*

$\min_{1\le i\le n-1}\{l_i\} = O(\epsilon^{-1/(p+1)})$, we can use the relations $P(l), G(l) \sim O(\epsilon)$. That is, based on a chosen small parameter ϵ, one can estimate the required minimum separation distance for which these conditions are satisfied. Figure 8 (a) shows an example of the function $P(l)$ and $G(l)$ for $(\delta, \mu, p_1, p_2) = (1, 1, 2, 2)$. In this case, we found that for $\epsilon = 0.1$ we should at least require $l_{min} > 5.7$.

We would also like to point out that the leading-order system obtained here, (4.10), has a crucial difference from the systems obtained for the description of pulse interactions in local equations (see, e.g., [16, 51, 55]). For local equations which have pulses with exponentially decaying tails, it is sufficient to take into account only the immediate neighbors for each pulse, whereas for nonlocal equations we have to include long-range interactions due to the algebraically decaying tails of the pulses.

Note that projections Π_k are well defined on, e.g., L^1 space. However, if we were to consider, for example, infinite arrays of pulses and the functions $\hat{u}$ that are not localized and therefore not integrable, we would need to introduce expansions of elements of a more generalized space into the spectrum of $\mathcal{L}_k^{adj}$ in the same way, for example, that the Fourier transform is introduced for the Schwartz class of tempered distributions $\mathcal{S}'(\mathbb{R})$. Unfortunately, the spectral theory for non–self-adjoint operators with nonconstant coefficients is not as complete as for self-adjoint operators, and we therefore do not consider such generalizations here.

Finally we note that (4.10) is derived based on the infinite domain pulses and is valid on the infinite domain. For pulses given on a periodic domain $[-L, L]$, on the other hand, similar equations can be obtained. Due to periodicity, for a given pulse we need to take into account the effect of the pulses that interact with the given pulse through the period. Thus, for periodic intervals, the system describing the dynamics of the pulses is (assuming $L > b(\epsilon)/2$, where $b(\epsilon)$ is defined below (4.10))

$$\dot{x}_k = \sum_{|x_i - x_k| < b(\epsilon)} P(x_i - x_k) + \sum_{|x_i - x_k| \ge 2L - b(\epsilon)} P(x_i - x_k + 2\,\mathrm{sgn}(x_i - x_k)L). \tag{4.11}$$

4.1. Two-pulse systems. As an example, we consider next a two-pulse system, $n = 2$. Based on (4.10) we obtain that the dynamics of the pulse locations is described by the system

$$\dot{x_1} = P(x_2 - x_1), \quad \dot{x_2} = P(x_1 - x_2), \tag{4.12}$$

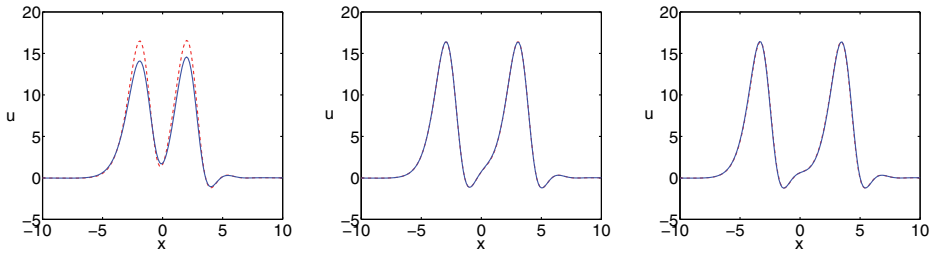

(a) $c^* = 5.15$, $l^* = 4.1(3.9)$. (b) $c^* = 5.868$, $l^* = 6.0(6.0)$. (c) $c^* = 5.879$, $l^* = 6.8(6.8)$.

FIG. 9. *(Color online.) Comparison between the theoretically predicted (dashed (red) lines) and the "true" (solid (blue) lines) bound states of the system for* $(\delta, \mu, p_1, p_2) = (1, 1, 2, 2)$. *The values in parentheses are the theoretically predicted separation distances that are used to construct the initial guess to compute the "true" bound states.*

which can be further simplified by introducing the separation distance $l = x_2 - x_1$,

$$\dot{l} = P(-l) - P(l). \tag{4.13}$$

Depending on the initial condition, the two pulses may attract ($P(-l) < P(l)$) or repel ($P(-l) > P(l)$) each other. As they get closer to or farther from each other, their velocity difference decreases until both pulses propagate at the same velocity, forming a bound state ($P(-l) = P(l)$). Figure 8(b) depicts the function $P(-l) - P(l)$ for $(\delta, \mu, p_1, p_2) = (1, 1, 2, 2)$. Bound states of the system are marked as dots and circles that represent stable and unstable equilibria, respectively. It is found that there exist only four possible bound states, two stable and two unstable. In fact, it can be shown that for nonlocal equations, $P(l)$ is algebraically decaying as $l \to \pm\infty$, and it can be concluded that there may exist only a finite number of bound states, unlike for local equations.

To validate the theoretically predicted bound states (zeros of (4.13)), we use $\bar{u} = u^*(x) + u^*(x + \bar{l})$, where $P(-\bar{l}) - P(\bar{l}) = 0$, as an initial guess to solve for the real bound states of the nonlocal model. The comparison for $(\delta, \mu, p_1, p_2) = (1, 1, 2, 2)$ is shown in Figure 9, where the theoretical predictions, $\bar{u}(x)$, are shown as dashed (red) lines, while the true bound states are shown as solid (blue) lines. It can be seen there is good agreement between the predictions and the true bound states, which becomes better for larger separation distances. Note that we do not show the comparison for the smallest predicted separation distance $l \approx 3$ in Figure 8(b), since the theory is only valid for pulses that are well-separated, and for $l \approx 3$ we do not find good agreement.

In Figure 10 we simulate the interaction of two pulses on the periodic domain $[-10, 10]$ for $(\delta, \mu, p_1, p_2) = (1, 1, 2, 2)$ and show the dynamics of the separation distance. We find that the theoretically predicted dynamics computed using (4.11) (dashed (red) lines) fits well with the true dynamics of model (1.1) (solid (blue) lines). Also, better agreement is found for larger separation distances, as expected.

It is known that for the gKS equation, two pulses repel each other for large enough separation distances when dispersion is sufficiently strong (see, e.g., [51]). As a result, for an array of pulses on a periodic domain, the solution with equal separation distances is always a fixed point. This is also the case for $(\delta, \mu, p_1, p_2) = (1, 1, 2, 2)$. We have verified that the function $P(-l) - P(l)$ approaches 0^+ as l increases, and therefore on the periodic domain $[-10, 10]$ two pulses that are far away initially will approach a state with separation distance $l = 10$. In Figure 10(a) it can be seen that

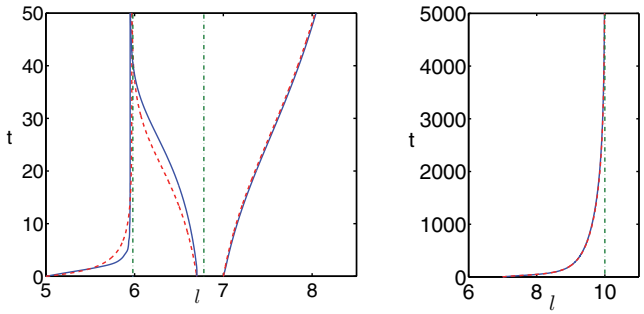

(a) (b)

FIG. 10. *(Color online.)* (a) *Interaction of two pulses on the periodic domain* $[-10, 10]$ *for* $(\delta, \mu, p_1, p_2) = (1, 1, 2, 2)$. *The solid (blue) lines correspond to the true dynamics obtained by numerically solving* (1.1)*, the dashed (red) lines are obtained by solving* (4.13)*, and the dash-dotted (green) lines correspond to the theoretical bound states. Panel* (b) *shows the long-time evolution for the pulses with the initial separation distance* $l = 7$.

the pulses with initial separation distance $l = 7$ repel each other and approach the state with $l = 10$; see Figure 10(b) for the long-time behavior.

However, for nonlocal equations, we find that two pulses do not always repel each other at sufficiently large separation distances. For a single-pulse solution of Case 2 in section 3.3 and under the condition that $p_2 \in (0, 1)$, the right tail is negative and the left tail is positive, which gives $P(l \gg 1) > 0$ and $P(-l \gg 1) < 0$, and the following result can be concluded: If $\delta = 0$ or $p_2 < p_1$ and $p_2 \in (0, 1)$, we have $P(-l) - P(l) < 0$ for $|l| \gg 1$, which implies that there exists a long-range attractive force so that if the separation distance between two pulses is sufficiently large, they attract each other and form a bound state with finite separation distance. Otherwise, the pulses repel each other.

Figure 11 corresponds to $(\delta, \mu, p_1, p_2) = (1, 1, 2, 0.9)$ that satisfies the above-mentioned conditions. It can be seen in Figure 11(a) that there exist five bound states, and the last one at $l \approx 9.5$ is stable. Pulses with larger separation distances will attract each other, and for pulses on the periodic domain, the equal-distance state is no longer stable. This is illustrated in Figure 11(b) showing the time evolution of the separation distances for two-pulse systems on the periodic domain $[-13, 13]$. It can be seen that the pulses attract each other even when the initial separation is $l = 12$ and form a bound state as predicted by the theory.

4.2. Multipulse systems. For an n-pulse system the evolution of the pulse locations can be described by (4.10), and the evolution of the separation distances is given by

$$\dot{l}_k = \dot{x}_{k+1} - \dot{x}_k. \tag{4.14}$$

Figure 12 shows an example of a four-pulse system on a periodic domain $[-20, 20]$. The true dynamics of the pulse locations and separation distances obtained by solving (1.1) is shown by solid (blue) lines in panels (a) and (b), respectively. Due to periodicity we have four separation distances with $l_4 = x_1 - x_4 + 40$. We also solve the reduced ordinary differential equation (ODE) system (4.11) using the same initial pulse locations. As discussed above, long-range interactions need to be taken into account for an accurate description of the dynamics. To illustrate this, we perform two

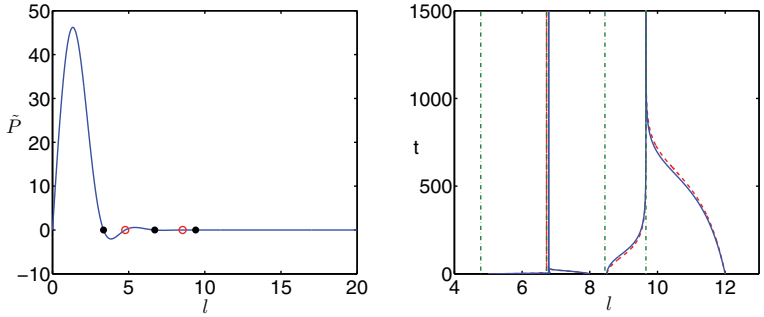

(a) $\tilde{P}(l) = P(-l) - P(l)$. (b)

FIG. 11. *(Color online.)* $(\delta, \mu, p_1, p_2) = (1, 1, 2, 0.9)$. (a) *Filled/empty circles indicate stable/unstable equilibria, respectively.* (b) *Evolution of the separation distances for two-pulse systems on the periodic domain* $[-13, 13]$. *The solid (blue) lines correspond to the true dynamics obtained by numerically solving* (1.1)*, the dashed (red) lines are obtained by solving* (4.13)*, and the dash-dotted (green) lines correspond to the theoretical bound states.*

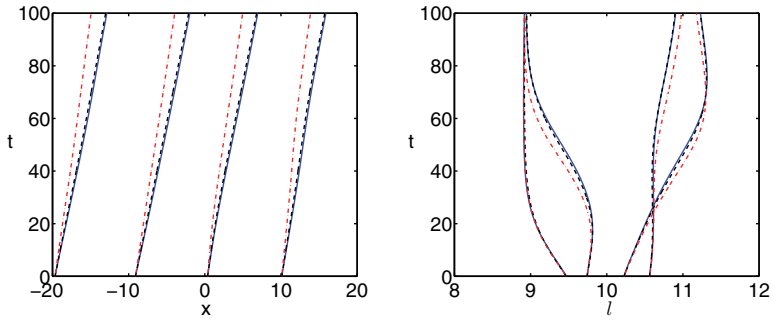

(a) Pulse locations. (b) Separation distances.

FIG. 12. *(Color online.) Interaction of two pulses on the periodic domain* $[-20, 20]$ *for* $(\delta, \mu, p_1, p_2) = (1, 1, 1, 2)$. *The solid (blue) lines are the pulse locations and separation distances extracted from the numerical solution of the PDE* (1.1). *The dash-dotted (red) lines and dashed (black) lines are obtained from the reduced ODE system* (4.13) *that takes into account two and six neighboring pulses, respectively.*

simulations: One takes into account only two neighboring pulses, one on the right and one on the left (the same as for the interaction of pulses for local equations), and the other takes into account six neighboring pulses, three on each side, shown as dash-dotted (red) lines and dashed (black) lines, respectively. It can be seen that we have much better agreement with the true dynamics when more neighboring pulses are taken into account.

5. Analysis of absolute and convective instability of a single-pulse solution. The regularizing effect of dispersion on the dynamics of the solutions of (1.1) can be associated with the fact that for sufficiently strong dispersion the pulses become convectively unstable and can tolerate localized disturbances, which are propagated upstream in the frame moving with the pulse velocity (see, e.g., [10, 51] for the discussion of absolute and convective instabilities of the pulses of the gKS equation). It is therefore pertinent to analyze the absolute and convective instability of a single pulse.

It should be noted that for local equations, a rather elegant way to analyze convective and absolute instabilities is by utilizing the exponentially weighted spaces approach; see, e.g., [44, 51]. For nonlocal equations, however, this approach is inapplicable. Here we adopt an approach similar to that of [17].

Let u^* be an infinite-domain pulse, and let η be a small perturbation. The linearized equation for η in the frame moving at velocity c^* of a single pulse is

$$\partial_t \eta = \mathcal{L}[\eta], \tag{5.1}$$

where $\mathcal{L}$ is the following linear operator:

$$\mathcal{L}[f] = c^* \partial_x f - \partial_x^2 f - \partial_x(\mathcal{N}[f]) - \partial_x^4 f - \partial_x(u^* f). \tag{5.2}$$

The solution of (5.1) can be written as (see, e.g., [11])

$$\eta(x,t) = \sum_i \mathrm{e}^{\lambda_i t} A_i \phi_i(x) + \int_\Sigma \mathrm{e}^{\sigma t} a(\sigma) \phi(x,\sigma)\, \mathrm{d}\sigma, \tag{5.3}$$

where the summation is over all the isolated eigenvalues λ_i with corresponding eigenfunctions $\phi_i(x)$ (in fact, for the given model, we find numerically that there is only one isolated eigenvalue, which is real and negative; see, e.g., [11, 51] for the case of the gKS equation), A_i are constants, Σ is the essential spectrum of $\mathcal{L}$ given by (4.5), and $\phi(x,\sigma)$ are the eigenfunctions of $\mathcal{L}$, i.e., the functions belonging to the null space of $\sigma I - \mathcal{L}$. Taking into account (4.5), (5.3) can be rewritten as

$$\eta(x,t) = \mathrm{e}^{\lambda_1 t} A_1 \phi_1(x) + \int_{-\infty}^{\infty} \mathrm{e}^{\sigma(\kappa) t} A(\kappa) \Phi(x,\kappa)\, \mathrm{d}\kappa, \tag{5.4}$$

where $A(\kappa) = a(\sigma(\kappa))\sigma'(\kappa)$, $\Phi(x,\kappa) = \phi(x,\sigma(\kappa))$. We note that $\sigma(-\kappa) = \overline{\sigma(\kappa)}$, where the overline denotes complex conjugation. Also, we can choose the eigenfunctions so that $\Phi(x,-\kappa) = \overline{\Phi(x,\kappa)}$, and for a real η we also have $A(-\kappa) = \overline{A(\kappa)}$. Due to $\lambda_1 < 0$, the first term decays to zero, and we analyze the integral term, which we denote by I. To clarify the nature of the instability, we wish to find out whether or not it is possible to deform the contour of integration so that it passes through the region where the real part of $\sigma(\kappa)$ is negative. However, $\sigma(\kappa)$ is not analytic at $\kappa = 0$ unless $\mathcal{N}$ is local. We cannot therefore directly apply the classical approach of Huerre and Monkewitz [22]. To overcome this, we first split the integral into two parts, and, using the properties of σ, A, and Φ, we obtain

$$\begin{aligned} I &= \int_{-\infty}^{0} \mathrm{e}^{\sigma(\kappa) t} A(\kappa) \Phi(x,\kappa)\, \mathrm{d}\kappa + \int_0^{\infty} \mathrm{e}^{\sigma(\kappa) t} A(\kappa) \Phi(x,\kappa)\, \mathrm{d}\kappa \\ &= \overline{\int_0^{\infty} \mathrm{e}^{\sigma(\kappa) t} A(\kappa) \Phi(x,\kappa)\, \mathrm{d}\kappa} + \int_0^{\infty} \mathrm{e}^{\sigma(\kappa) t} A(\kappa) \Phi(x,\kappa)\, \mathrm{d}\kappa = 2\,\mathrm{Re}(K(x,t)), \end{aligned} \tag{5.5}$$

where $K(x,t) = \int_0^{\infty} \mathrm{e}^{\sigma(\kappa) t} A(\kappa) \Phi(x,\kappa)\, \mathrm{d}\kappa$. In the latter integral, $\sigma(\kappa)$ can be replaced by the function $\sigma_+(\kappa) = \mathrm{i}\, c^* \kappa + \kappa^2 + \mathrm{i}\, \delta \kappa^{p_1+1} + \mu \kappa^{p_2+1} - \kappa^4$ that is analytic in the whole complex plane (except for a branch cut if p_1 or p_2 is not an integer). We note that for sufficiently large μ there exist two roots $0 \le \kappa_1 < \kappa_2$ of $\mathrm{Re}(\sigma_+(\kappa))$ so that $\mathrm{Re}(\sigma_+(\kappa))$ is positive for $\kappa \in (\kappa_1, \kappa_2)$ and negative for other positive values of κ. It is therefore sufficient to consider the behavior of the integral from κ_1 to κ_2, $K_1(x,t) = \int_{\kappa_1}^{\kappa_2} \mathrm{e}^{\sigma_+(\kappa) t} A(\kappa) \Phi(x,\kappa)\, \mathrm{d}\kappa$. The nature of instability now depends on the

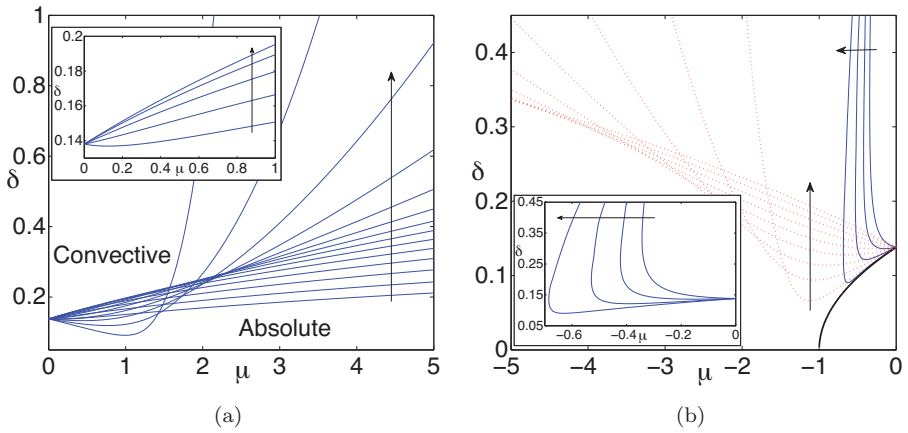

FIG. 13. *(Color online.) The boundaries separating the absolute and convective instability regions in the* (μ, δ)*-plane for* $p_1 = 2$*. Panel* (a) *corresponds to* $\mu > 0$*, and* p_2 *is changing from* 0.2 *to* 2.8 *with the step size* 0.2 *(the arrows indicate the directions of increasing* p_2*). The inset shows a zoom of the region near* $\mu = 0$*, and the boundaries are shown for* p_2 *changing form* 0.2 *to* 1 *with the step size* 0.2*. Panel* (b) *corresponds to* $\mu < 0$*. The thin solid lines correspond to* p_2 *taking the values from* 0.2 *to* 0.8 *with the step size* 0.2*. The thick solid line corresponds to* $p_2 = 1$*. The dotted lines correspond to* p_2 *taking the values from* 1.2 *to* 2.8 *with the step size* 0.2 *(the arrows indicate the directions of increasing* p_2*). The inset shows a zoom of the region near* $\mu = 0$*.*

topology of the curves in the complex κ-plane given by the equation $\mathrm{Re}(\sigma_+(\kappa)) = 0$. If it is possible to connect the point $(\kappa_1, 0)$ with the point $(\kappa_2, 0)$ by a curve along which $\mathrm{Re}(\sigma_+(\kappa))$ vanishes, then the instability is convective. In such a case, there exists a saddle point of $\mathrm{Re}(\sigma_+(\kappa))$ at which $\mathrm{Re}(\sigma_+(\kappa)) < 0$. Then it is possible to deform the integration contour in K_1 into the steepest descent path passing through the saddle point in the region where $\mathrm{Re}(\sigma_+(\kappa)) < 0$. The instability is then seen to decay at each fixed point in space. Otherwise, the contour of integration can be deformed into the steepest descent path passing through the saddle point of $\mathrm{Re}(\sigma_+(\kappa))$ at which $\mathrm{Re}(\sigma_+(\kappa))$ is positive. In such a case, $|K_1(x,t)|$ grows as t increases at a fixed value of x, and the instability is absolute. We can see, therefore, that the change from one instability type to another happens when the two different branches of the curves $\mathrm{Re}(\sigma_+(\kappa)) = 0$ are pinched together at the saddle point. This implies the conditions $\mathrm{Re}(\sigma_+(\kappa)) = 0$ and $\mathrm{d}(\sigma_+(\kappa))/\mathrm{d}\kappa = 0$.

Figure 13 shows the boundaries in the (μ, δ)-plane separating the regions of absolute and convective instabilities for $p_1 = 2$. Panels (a) and (b) correspond to positive and negative values of μ, respectively. Such boundaries are computed by continuation by solving (3.2) together with the conditions $\mathrm{Re}(\sigma_+(\kappa)) = 0$ and $\mathrm{d}(\sigma_+(\kappa))/\mathrm{d}\kappa = 0$. In Figure 13(a), $\mu > 0$, and p_2 takes the values from 0.2 to 2.6 with the step size equal to 0.2 (the direction of increasing p_2 is indicated by the arrow). The inset shows a zoom of the region near $\mu = 0$, and the boundaries are shown for $p_2 = 0.2$, 0.4, 0.6, 0.8, and 1. We can observe that if p_2 is sufficiently small (e.g., $p_2 = 0.2$), when increasing μ the boundary first goes slightly down (as can be seen in the inset) and then monotonically increases. For larger values of p_2 (e.g., for $p_2 = 1$), the boundary does not go down initially but monotonically increases from the beginning, meaning that for larger values of μ stronger dispersion is needed to regularize the dynamics. When p_2 becomes even larger (e.g., $p_2 = 2.8$), we can observe again that the boundary

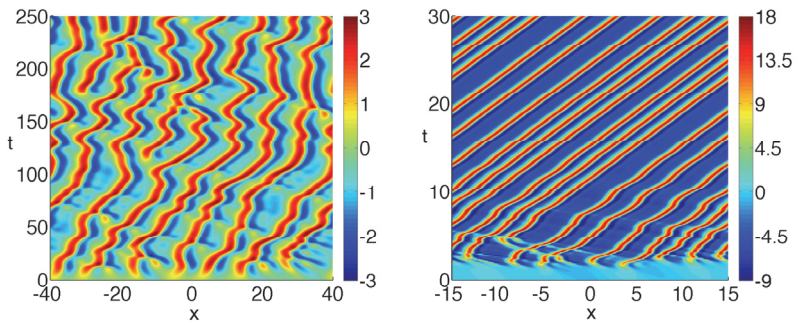

(a) $\mu = 0$. (b) $\mu = 1$, $p_2 = 2.95$.

FIG. 14. *(Color online.) Spatio-temporal dynamics of* (1.1) *with* $\delta = 0.13$ *and* $p_1 = 2$.

first goes down but then rapidly goes up. Interestingly, the fact that the boundary first goes down for a sufficiently small or a sufficiently large value of p_2 means that initially the destabilizing term with that value of p_2 should have a regularizing effect on the dynamics. This effect is demonstrated in Figure 14 showing the contour plots of u corresponding to the time evolution for $\delta = 0.13$ and $p_1 = 2$. Figure 14(a) corresponds to $\mu = 0$ (for which a pulse solution is expected to be absolutely unstable), whereas Figure 14(b) corresponds to $\mu = 1$ and $p_2 = 2.95$ (for which the pulse solution is expected to be convectively unstable). We note that for convenience of presentation the time evolution in panel (b) is shown in a frame moving at velocity 1. The solutions are computed using as an initial condition a small-amplitude randomly generated disturbance added to the flat state $u = 0$. The spatial intervals are $[-40, 40]$ and $[-15, 15]$ for Figures 14(a) and (b), respectively. In Figure 14(a), when the destabilizing nonlocal term is absent, we can observe that the dynamics is irregular, while in Figure 14(b) we see that the introduction of the destabilizing nonlocal term regularizes the dynamics —the solution evolves into an array of pulses.

For the results for $\mu < 0$ shown in Figure 13(b), the thin solid (blue) lines correspond to p_2 taking the values from 0.2 to 0.8 with the step size 0.2, the thick solid (black) line corresponds to $p_2 = 1$, and the dotted (red) lines correspond to p_2 taking the values from 1.2 to 2.8 with the step size 0.2. The directions of increasing p_2 are indicated by the arrows. It can be easily verified that for $p_2 < 1$, there is no linear instability of the flat state if $\mu < \mu_c = k_c^{3-p_2} - k_c^{1-p_2}$, where $k_c = [(1-p_2)/(3-p_2)]^{1/2}$. We therefore do not expect nonlinear waves to exist for $\mu < \mu_c$. Indeed, in the inset, showing a zoom of the region near $\mu = 0$, it can be observed that the lines corresponding to $p_2 < 1$ have turning points. It should be noted, however, that the upper parts of these curves correspond to small-amplitude, slow waves that are not observed in time-dependent computations. As a result, we conclude that the regions below the lower parts of these curves correspond to absolute instability, whereas the regions above the lower parts of these curves correspond to convective instability. The curve for $p_2 = 1$ terminates at $\mu = -1$ below which there is no linear instability. The curves corresponding to $p_2 > 1$ can be continued to arbitrary negative values of μ. For sufficiently large values of μ (e.g., for $\mu = 2.8$) we can observe that the absolute-convective instability boundary monotonically increases as μ decreases. This means that introducing a stabilizing term with such a p_2 should have a deregularizing effect on the dynamics. For intermediate values of p_2, we can see that the

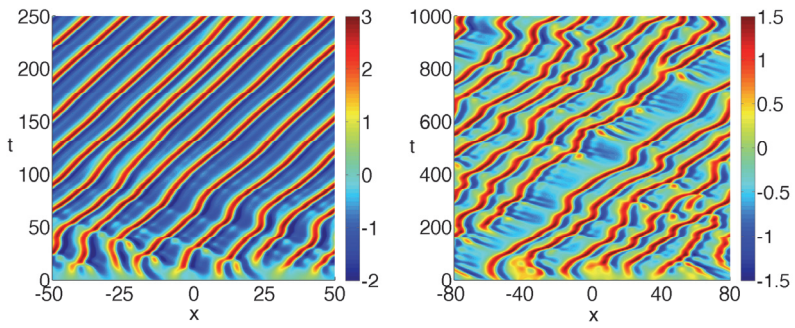

(a) $\mu = 0$. (b) $\mu = -2$, $p_2 = 2.95$.

FIG. 15. *(Color online.) Spatio-temporal dynamics of* (1.1) *with* $\delta = 0.25$ *and* $p_1 = 2$.

absolute-convective instability boundary first goes down as μ decreases, but then goes up (except for $p_2 \leq 1$). This means that introducing a stabilizing term with such a p_2 initially has a regularizing effect on the dynamics but then again has a deregularizing effect. This deregularizing effect of a stabilizing term is demonstrated in Figure 15 for $\delta = 0.25$ and $p_1 = 2$. Figure 15(a) corresponds to $\mu = 0$ (for which a pulse solution is expected to be convectively unstable), whereas Figure 15(b) corresponds to $\mu = -2$ and $p_2 = 2.95$ (for which the pulse solution is expected to be absolutely unstable). The solutions are computed using as an initial condition a small-amplitude randomly generated disturbance added to the flat state $u = 0$. The spatial intervals are $[-50, 50]$ and $[-80, 80]$ for Figures 15(a) and (b), respectively. In Figure 15(a), when the destabilizing nonlocal term is absent, we observe that the dynamics is quite regular, while in Figure 15(b), we observe that the introduction of the stabilizing nonlocal term indeed deregularizes the dynamics.

6. Conclusions. We have studied coherent structures in nonlocal dispersive active-dissipative nonlinear systems. As a prototype, we used the KS equation with an additional nonlocal term in the form of a pseudodifferential operator, having stabilizing/destabilizing and dispersive parts. As for the gKS equation, time-dependent simulations showed that sufficiently strong dispersion regularizes the chaotic behavior of the solutions, which evolve into arrays of interacting pulses that can form bound states. We analyzed the asymptotic characteristics of such coherent structures. In particular, we showed that in the large dispersion limit the pulse shape and speed are proportional to the dispersion parameter. We analyzed how the proportionality factors depend on the other parameters of the equation. In the limit when the destabilizing effect of the nonlocal term becomes large, we analyzed the pulse characteristics by scaling arguments and found that the spatial scale, pulse shape, and speed depend on the destabilizing parameter. In addition, we showed that the tails of the pulses tend to zero algebraically (and not exponentially as for the gKS equation), and we analyzed the dependence of the rate of this decay on the parameters of the equation.

We further developed a weak-interaction theory of the coherent structures. By representing the solution as a superposition of pulses and an overlap function and projecting the dynamics onto the translational modes, we derived a system of ODEs describing the dynamics of the pulse locations. For nonlocal equations we have to include long-range interactions for an accurate description of the dynamics, in contrast to local equations, where it is sufficient to take into account only the immediate

neighbors for each pulse. In addition, we found that in certain cases there may exist long-range attractive forces between the pulses, unlike with the gKS equation, which is something that has been also observed experimentally in optical solitons [43]. We then compared the interaction theory with numerical simulations of the full equation and found very good agreement. We also analyzed bound states of the pulses. Since the Shilnikov-type approach is not applicable to nonlocal equations, we obtained bound states by analyzing the fixed points of the reduced ODE system. The number of possible bound states for fixed parameter values is always finite, unlike that for local equations.

Finally, to analyze the regularizing effect of the nonlocal term, we studied absolute and convective instabilities of single-pulse solutions. The classical analysis of Huerre and Monkewitz [22] is not applicable in our case; instead, we adopted an approach similar to that of [17] and obtained the boundaries in the parameter spaces separating the absolute and convective instability regions. As expected, by increasing the strength of the dispersion term, a single-pulse solution undergoes a transition from absolute to convective instability. On the other hand, we found that stabilization/destabilization does not necessarily imply regularization/deregularization of the dynamics; namely, there are parameter regions where adding stabilization/destabilization may move a single-pulse solution from the convective/absolute instability region to the absolute/convective instability region. These findings were corroborated by time-dependent simulations of the full equation.

Appendix A. Properties of $\mathcal{N}_1$ and $\mathcal{N}_2$. Recall that $\mathcal{F}[\mathcal{N}_1[f]] = n_1(k)\,\hat{f}(k)$ and $\mathcal{F}[\mathcal{N}_2[f]] = \mathrm{i}\,n_2(k)\,\hat{f}(k)$, where $n_1(k)$ and $n_2(k)$ are even and odd real-valued functions, respectively. Here the hats and $\mathcal{F}$ denote the Fourier transforms. We use the following definitions of the Fourier and inverse Fourier transforms:

(A.1)
$$\hat{f}(k) = \mathcal{F}[f](k) = \int_{-\infty}^{\infty} f(x)\mathrm{e}^{-\mathrm{i}kx}\,\mathrm{d}x, \qquad f(x) = \mathcal{F}^{-1}[\hat{f}](x) = \frac{1}{2\pi}\int_{-\infty}^{\infty} \hat{f}(k)\mathrm{e}^{\mathrm{i}kx}\,\mathrm{d}k.$$

Using Parseval's theorem, we can prove the following properties:

1. $\langle \mathcal{N}_1[f],\, g\rangle = \langle f,\, \mathcal{N}_1[g]\rangle$. That is, $\mathcal{N}_1$ is self-adjoint, $\mathcal{N}_1^{adj} = \mathcal{N}_1$.
2. $\langle \mathcal{N}_2[f],\, g\rangle = -\langle f,\, \mathcal{N}_2[g]\rangle$. That is, $\mathcal{N}_2$ is anti-self-adjoint, $\mathcal{N}_2^{adj} = -\mathcal{N}_2$.
3. $\langle \mathcal{N}_1[f],\, \partial_x f\rangle = 0$.
4. $\langle \mathcal{N}_2[f],\, \partial_x f\rangle > 0$ for a nonconstant function f.

Appendix B. The null space of $\mathcal{L}^{adj}$. Let $\mathcal{L}$ be the operator linearized about the pulse shape u^*; see (5.2). The formal adjoint of $\mathcal{L}$ is

(B.1)
$$\mathcal{L}^{adj}[f] = -c^*\,\partial_x f - \partial_x^2 f + \delta\mathcal{N}_1[\partial_x f] - \mu\mathcal{N}_2[\partial_x f] - \partial_x^4 f + u^*\partial_x f.$$

To analyze the spectra of these operators on the infinite domain, it is appropriate to consider them on a periodic domain $[-L, L]$ and take the limit $L \to \infty$; see [44]. As has been discussed in section 4, on a periodic domain zero is an eigenvalue of $\mathcal{L}$ and $\mathcal{L}^{adj}$ of algebraic and geometric multiplicities 2 and 1, respectively. The eigenfunction and the generalized eigenfunction are $\partial_x u^*$ and -1 and correspond to the translational and Galilean invariance of the equation, respectively. The adjoint eigenfunction is a constant. We choose it to be $-1/(2L)$ so that its inner product with -1 is unity. The generalized adjoint eigenfunction, on the other hand, does not have an analytical expression and needs to be found numerically. Let us denote it by Ψ, so that $\mathcal{L}^{adj}[\Psi] = -1/(2L)$ on the periodic domain $[-L, L]$. It is easy to check that the normalization

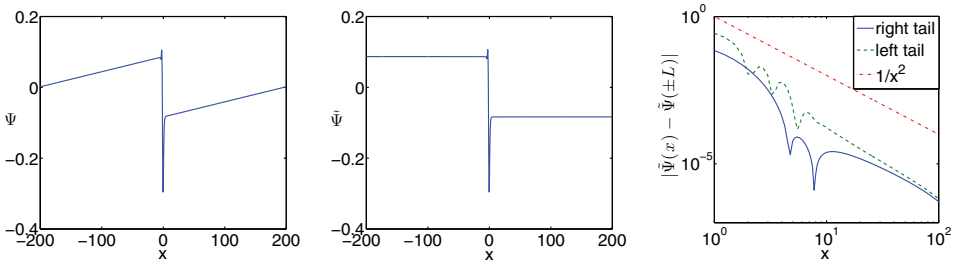

(a) (b) (c)

FIG. 16. *The functions* (a) Ψ *and* (b) $\tilde{\Psi}$ *for* $(\delta, \mu, p_1, p_2) = (1, 1, 2, 2)$ *on the periodic domain* $[-200, 200]$. (c) *The right and left tails of* $\tilde{\Psi}$ *defined as* $|\tilde{\Psi}(x) - \tilde{\Psi}(\pm L)|$ *are shown on a log-log scale.*

condition, $\int_{-L}^{L} \Psi \partial_x u^* dx = 1$, holds automatically. We further require that $\int_{-L}^{L} \Psi dx = 0$, so that it is orthogonal to the generalized zero-eigenfunction of $\mathcal{L}$. Figure 16(a) shows an example of the function Ψ for $(\delta, \mu, p_1, p_2) = (1, 1, 2, 2)$ when $L = 200$. To analyze the function Ψ, we first note that its derivative, $\psi = \partial_x \Psi$, satisfies

$$-c^* \psi - \partial_x \psi + \delta \mathcal{N}_1[\psi] - \mu \mathcal{N}_2[\psi] - \partial_x^3 \psi + u^* \psi = -\frac{1}{2L}. \tag{B.2}$$

Since u^* decays to zero for large $|x|$, the function ψ should approach $1/(2c^*L)$ for large $|x|$. Let us rewrite ψ as $\tilde{\psi} + 1/(2c^*L)$, so that $\tilde{\psi}$ tends to zero for large $|x|$. Then (B.2) becomes

$$-c^* \tilde{\psi} - \partial_x \tilde{\psi} + \delta \mathcal{N}_1[\tilde{\psi}] - \mu \mathcal{N}_2[\tilde{\psi}] - \partial_x^3 \tilde{\psi} + u^* \left(\tilde{\psi} + \frac{1}{2c^*L} \right) = 0. \tag{B.3}$$

By integrating (B.3) over the domain $[-L, L]$ we find

$$\int_{-L}^{L} \tilde{\psi} \, \mathrm{d}x = -\frac{1}{c^*}. \tag{B.4}$$

Then using the same argument as in section 3.3 we can conclude that

$$\psi(x) \sim \frac{1}{2c^*L} + O\left(\frac{1}{|x|^{p+1}} \right). \tag{B.5}$$

Figure 17 shows the function ψ in panel (a) and the asymptotic behavior of the tails that are obtained numerically for $(\delta, \mu, p_1, p_2) = (1, 1, 2, 2)$ in panel (b). Excellent agreement with the analysis is found.

Next, we write $\Psi = \tilde{\Psi} + x/(2c^*L)$, where $\partial_x \tilde{\Psi} = \tilde{\psi}$ and therefore $\tilde{\Psi}(L) - \tilde{\Psi}(-L) = -1/c^*$ (i.e., $\tilde{\Psi}$ attains two different constants at the two boundaries); see Figure 16(b) showing $\tilde{\Psi}$ for $(\delta, \mu, p_1, p_2) = (1, 1, 2, 2)$ when $L = 200$. By combining these facts with (B.5), we obtain, for large $|x|$,

$$\Psi(x) \sim \frac{x}{2c^*L} + \tilde{\Psi}(\pm L) + O\left(\frac{1}{|x|^p} \right). \tag{B.6}$$

Figure 16(c) shows the scaling law of the right and left tails of $\tilde{\Psi}$ for $(\delta, \mu, p_1, p_2) = (1, 1, 2, 2)$, and the $O(1/x^2)$ behavior of the tails can be confirmed as predicted by (B.6).

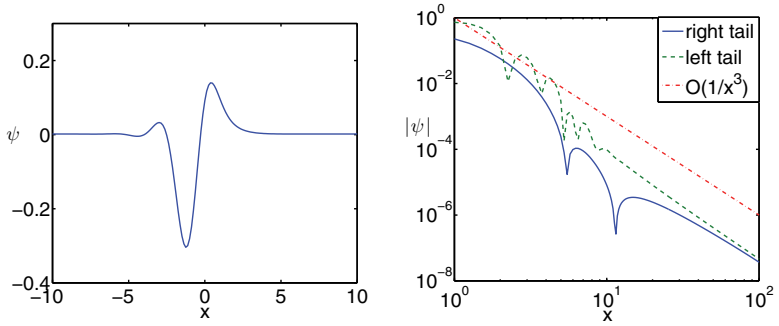

(a) ψ. (b) Right and left tails of ψ.

FIG. 17. *The functions ψ for $(\delta, \mu, p_1, p_2) = (1, 1, 2, 2)$. The right and left tails are defined as $|\psi(\pm x) - 1/(2c^* L)|$.*

Finally, we comment on the limit $L \to \infty$. In such a limit, we find that $\psi \sim O\left(1/|x|^{p+1}\right)$ as $|x| \to \infty$ and $\Psi \sim \mp 1/(2c^*) + O\left(1/|x|^p\right)$ as $x \to \pm\infty$. Moreover, the function Ψ is in the null space of the adjoint operator.

REFERENCES

[1] L. ABDELOUHAB, J. L. BONA, M. FELLAND, AND J.-C. SAUT, *Nonlocal models for nonlinear dispersive waves*, Phys. D, 40 (1989), pp. 360–392.

[2] G. AKRIVIS, D. T. PAPAGEORGIOU, AND Y.-S. SMYRLIS, *Computational study of the dispersively modified Kuramoto–Sivashinsky equation*, SIAM J. Sci. Comput., 34 (2012), pp. A792–A813.

[3] G. AKRIVIS, D. T. PAPAGEORGIOU, AND Y.-S. SMYRLIS, *On the analyticity of certain dissipative–dispersive systems*, Bull. Lond. Math. Soc., 45 (2013), pp. 52–60.

[4] N. J. ARMSTRONG, K. J. PAINTER, AND J. A. SHERRATT, *A continuum approach to modelling cell-cell adhesion*, J. Theoret. Biol., 243 (2006), pp. 98–113.

[5] N. J. BALMFORTH, *Solitary waves and homoclinic orbits*, Annu. Rev. Fluid Mech., 27 (1995), pp. 335–373.

[6] B. BARKER, M. A. JOHNSON, P. NOBLE, L. M. RODRIGUES, AND K. ZUMBRUN, *Nonlinear modulational stability of periodic traveling-wave solutions of the generalized Kuramoto–Sivashinsky equation*, Phys. D, 258 (2013), pp. 11–46.

[7] A. P. BASSOM, M. G. BLYTH, AND D. T. PAPAGEORGIOU, *Nonlinear development of two–layer Couette–Poiseuille flow in the presence of surfactant*, Phys. Fluids, 22 (2010), 102102.

[8] T. B. BENJAMIN, *Internal waves of permanent form in fluids of great depth*, J. Fluid Mech., 29 (1967), pp. 559–592.

[9] H. C. CHANG AND E. A. DEMEKHIN, *Complex Wave Dynamics on Thin Films*, Elsevier, New York, 2002.

[10] H.-C. CHANG, E. A. DEMEKHIN, AND D. I. KOPELEVICH, *Stability of a solitary pulse against wave packet disturbances in an active medium*, Phys. Rev. Lett., 75 (1995), pp. 1747–1750.

[11] H.-C. CHANG, E. A. DEMEKHIN, AND D. I. KOPELEVICH, *Local stability theory of solitary pulses in an active medium*, Phys. D, 97 (1996), pp. 353–375

[12] M. CHUGUNOVA AND D. PELINOVSKY, *Two-pulse solutions in the fifth-order KDV equation: Rigorous theory and numerical approximations*, Discrete Contin. Dyn. Syst. Ser. B, 8 (2007), pp. 773–800.

[13] E. B. DAVIES, *Linear Operators and Their Spectra*, Cambridge Stud. Adv. Math. 106, Cambridge University Press, Cambridge, UK, 2007.

[14] A. DIDDENS AND S. J. LINZ, *Redeposition during ion-beam erosion can stabilize well-ordered nanostructures*, Europhys. Lett., 104 (2013), 17010.

[15] E. J. DOEDEL AND B. E. OLDEMAN, *AUTO07p: Continuation and Bifurcation Software for Ordinary Differential Equations*, Technical report, Concordia University, Montreal, 2012.

[16] C. DUPRAT, F. GIORGIUTTI-DAUPHINÉ, D. TSELUIKO, S. SAPRYKIN, AND S. KALLIADASIS, *Liquid film coating a fiber as a model system for the formation of bound states in active dispersive–dissipative nonlinear media*, Phys. Rev. Lett., 103 (2009), 234501.

[17] A. S. Fokas and D. T. Papageorgiou, *Absolute and convective instability for evolution PDEs on the half-line*, Stud. Appl. Math., 114 (2005), pp. 95–114.
[18] U. Frisch, Z.-S. She, and O. Thual, *Viscoelastic behaviour of cellular solutions to the Kuramoto–Sivashinsky model*, J. Fluid Mech., 168 (1986), pp. 221–240.
[19] P. Glendinning and C. Sparrow, *Local and global behavior near homoclinic orbits*, J. Statist. Phys., 35 (1984), pp. 645–696.
[20] J. A. González, S. Jiménez, A. Bellorin, L. E. Guerrero, and L. Vázquez, *Internal degrees of freedom, long-range interactions and nonlocal effects in perturbed Klein–Gordon equations*, Phys. A, 391 (2012), pp. 515–527.
[21] G. M. Homsy, *Model equations for wavy viscous film flow*, in Nonlinear Wave Motion, Lectures Appl. Math. 15, American Mathematical Society, Providence, RI, 1974, pp. 191–194.
[22] P. Huerre and P. A. Monkewitz, *Local and global instabilities in spatially developing flows*, Annu. Rev. Fluid Mech., 22 (1990), pp. 473–537.
[23] R. S. Johnson, *Shallow water waves on a viscous fluid—the undular bore*, Phys. Fluids, 15 (1972), pp. 1693–1699.
[24] R. S. Johnson, *A Modern Introduction to the Mathematical Theory of Water Waves*, Cambridge University Press, Cambridge, UK, 1997.
[25] S. Kalliadasis, E. A. Demekhin, C. Ruyer-Quil, and M. G. Velarde, *Thermocapillary instability and wave formation on a film falling down a uniformly heated plane*, J. Fluid Mech., 492 (2003), pp. 303–338.
[26] S. Kalliadasis, C. Ruyer-Quil, B. Scheid, and M. G. Velarde, *Falling Liquid Films*, Springer Ser. Appl. Math. Sci., Springer, London, 2012.
[27] Q. D. Katatbeh and P. J. Torres, *Existence of periodic and solitary waves for a nonlinear Schrödinger equation with nonlocal integral term of convolution type*, Commun. Nonlinear Sci. Numer. Simul., 18 (2013), pp. 1136–1142.
[28] T. Kawahara, *Formation of saturated solitons in a nonlinear dispersive system with instability and dissipation*, Phys. Rev. Lett., 51 (1983), pp. 381–383.
[29] T. Kawahara and S. Toh, *Pulse interactions in an unstable dissipative-dispersive nonlinear system*, Phys. Fluids, 31 (1988), pp. 2103–2111.
[30] Y. Kuramoto, *Diffusion-induced chaos in reaction systems*, Prog. Theor. Phys. Suppl., 64 (1978), pp. 346–367.
[31] M. J. Lighthill, *An Introduction to Fourier Analysis and Generalised Functions*, Cambridge University Press, Cambridge, UK, 1958.
[32] S. P. Lin, *Finite amplitude side-band stability of a viscous film*, J. Fluid Mech., 63 (1974), pp. 417–429.
[33] T.-S. Lin, D. Tseluiko, and S. Kalliadasis, *Numerical study of a non-local weakly nonlinear model for a liquid film sheared by a turbulent gas*, Procedia IUTAM, 11 (2014), pp. 98–109.
[34] R. Metzler and J. Klafter, *The random walk's guide to anomalous diffusion: A fractional dynamics approach*, Phys. Rep., 339 (2000), pp. 1–77.
[35] J. W. Miles, *Korteweg–de Vries equation modified by viscosity*, Phys. Fluids, 19 (1976), p. 1063.
[36] A. A. Nepomnyashchy, *Stability of wave regimes in a film flowing down an inclined plane*, Fluid Dyn., 9 (1974), pp. 354–359.
[37] M. Nicoli, R. Cuerno, and M. Castro, *Unstable nonlocal interface dynamics*, Phys. Rev. Lett., 102 (2009), 256102.
[38] D. T. Papageorgiou, C. Maldarelli, and D. S. Rumschitzki, *Nonlinear interfacial stability of core-annular film flows*, Phys. Fluids A, 2 (1990), pp. 340–352.
[39] M. Pradas, S. Kalliadasis, P.-K. Nguyen, and V. Bontozoglou, *Bound-state formation in interfacial turbulence: Direct numerical simulations and theory*, J. Fluid Mech., 716 (2013), R2.
[40] M. Pradas, S. Kalliadasis, and D. Tseluiko, *Binary interactions of solitary pulses in falling liquid films*, IMA J. Appl. Math., 77 (2012), pp. 408–419.
[41] M. Pradas, D. Tseluiko, and S. Kalliadasis, *Rigorous coherent-structure theory for falling liquid films: Viscous dispersion effects on bound-state formation and self-organization*, Phys. Fluids, 23 (2011), 044104.
[42] M. Pradas, D. Tseluiko, C. Ruyer-Quil, and S. Kalliadasis, *Pulse dynamics in a power-law falling film*, J. Fluid Mech., 747 (2014), pp. 460–480.
[43] C. Rotschild, B. Alfassi, O. Cohen, and M. Segev, *Long-range interactions between optical solitons*, Nature Phys., 2 (2006), pp. 769–774.
[44] B. Sandstede and A. Scheel, *Absolute and convective instabilities of waves on unbounded and large bounded domains*, Phys. D, 145 (2000), pp. 233–277.
[45] D. Schertzer, M. Larchevêque, J. Duan, V. V. Yanovsky, and S. Lovejoy, *Fractional Fokker–Planck equation for nonlinear stochastic differential equations driven by non-*

Gaussian Levy stable noises, J. Math. Phys., 42 (2001), pp. 200–212.
[46] E. Simbawa, P. C. Matthews, and S. M. Cox, *Nikolaevskiy equation with dispersion*, Phys. Rev. E, 81 (2010), 036220.
[47] G. I. Sivashinsky, *Nonlinear analysis of hydrodynamic instability in laminar flames.* I. *Derivation of basic equations*, Acta Astronaut., 4 (1977), pp. 1177–1206.
[48] R. Smith, *Nonlinear Kelvin and continental–shelf waves*, J. Fluid Mech., 52 (1972), pp. 379–391.
[49] Y.-S. Smyrlis and D. T. Papageorgiou, *The effects of generalized dispersion on dissipative dynamical systems*, Appl. Math. Lett., 11 (1998), pp. 93–99.
[50] D. Tseluiko and S. Kalliadasis, *Nonlinear waves in counter-current gas–liquid film flow*, J. Fluid Mech., 673 (2011), pp. 19–59.
[51] D. Tseluiko and S. Kalliadasis, *Weak interaction of solitary pulses in active dispersive–dissipative nonlinear media*, IMA J. Appl. Math., 79 (2014), pp. 274–299.
[52] D. Tseluiko and D. T. Papageorgiou, *A global attracting set for nonlocal Kuramoto–Sivashinsky equations arising in interfacial electrohydrodynamics*, European J. Appl. Math., 17 (2006), pp. 677–703.
[53] D. Tseluiko and D. T. Papageorgiou, *Wave evolution on electrified falling films*, J. Fluid Mech., 556 (2006), pp. 361–386.
[54] D. Tseluiko and D. T. Papageorgiou, *Dynamics of an electrostatically modified Kuramoto–Sivashinsky–Korteweg–de Vries equation arising in falling film flows*, Phys. Rev. E (3), 82 (2010), 016322.
[55] D. Tseluiko, S. Saprykin, C. Duprat, F. Giorgiutti-Dauphiné, and S. Kalliadasis, *Pulse dynamics in low-Reynolds-number interfacial hydrodynamics: Experiments and theory*, Phys. D, 239 (2010), pp. 2000–2010.
[56] D. Tseluiko, S. Saprykin, and S. Kalliadasis, *Interaction of solitary pulses in active dispersive–dissipative media*, Proc. Est. Acad. Sci., 59 (2010), pp. 139–144.
[57] M. G. Velarde, *Solitons as dissipative structures*, Int. J. Quantum Chem., 98 (2004), p. 272–280.
[58] R. Vellingiri, D. Tseluiko, N. Savva, and S. Kalliadasis, *Dynamics of a liquid film sheared by a co-flowing turbulent gas*, Int. J. Multiphase Flow, 56 (2013), pp. 93–104.
[59] G. Z. Voyiadjis and R. K. Abu Al-Rub, *Nonlocal gradient-dependent thermodynamics for modeling scale-dependent plasticity*, Int. J. Mul. Comp. Eng., 5 (2007), pp. 295–323.
[60] H.-H. Wei, *Shear-flow and thermocapillary interfacial instabilities in a two-layer viscous flow*, Phys. Fluids, 18 (2006), 064109.
[61] G. B. Whitham, *Linear and Nonlinear Waves*, Wiley-Interscience, New York, 1974.